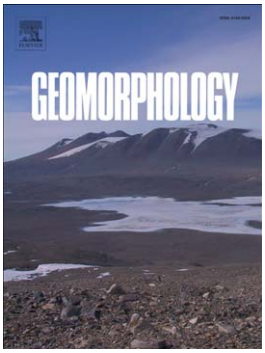

Modelling of estuarine response to sea-level rise during the Holocene: Application to the Guadiana Estuary - SW Iberia

D.M.R. Sampath, T. Boski, C. Loureiro, C. Sousa

PII: S0169-555X(15)00002-1
DOI: doi: 10.1016/j.geomorph.2014.12.037
Reference: GEOMOR 5043

To appear in: *Geomorphology*

Received date: 18 June 2014
Revised date: 24 December 2014
Accepted date: 31 December 2014

Please cite this article as: Sampath, D.M.R., Boski, T., Loureiro, C., Sousa, C., Modelling of estuarine response to sea-level rise during the Holocene: Application to the Guadiana Estuary - SW Iberia, *Geomorphology* (2015), doi: 10.1016/j.geomorph.2014.12.037

Modelling of estuarine response to sea-level rise during the Holocene: Application to the Guadiana Estuary - SW Iberia

D.M.R. Sampath[1]*, T. Boski[1], C. Loureiro[1,2,3], C. Sousa[1]

1 – CIMA- Centro de Investigação Marinha e Ambiental, Universidade do Algarve, Campus de Gambelas, 8005-139 Faro, Portugal. Corresponding author: rmudiyanselage@ualg.pt

2 – Environmental Sciences Research Institute, School of Environmental Sciences, University of Ulster, BT52 1SA Coleraine, Northern Ireland, UK

3 – Geological Sciences, School of Agriculture, Earth and Environmental Sciences, University of KwaZulu-Natal, Westville Campus, Durban, South Africa

Abstract

This paper focuses on simulations of the morphological evolution of an estuary during sedimentary infilling that accompanied Holocene sea-level rise. The simulations were conducted using the Estuarine Sedimentation Model, which uses a behaviour-oriented approach, supported by the chronostratigraphy of the estuary's sedimentary sequence. Behaviour curves were computed to represent the relationship between the estuarine channel depth below maximum high tide and the net accretion at a given location relative to the average sedimentation rate of the estuary during the Holocene. The model was validated by comparing the observed present-day bathymetry of the Guadiana River Estuary, southeastern Portugal, with the corresponding simulated bathymetries for nine control sections across the estuary. The best fit between simulated and actual sediment surface elevations was obtained along the cross-sections in the sheltered, low-energy environments of the estuary. The

accuracy of the sedimentary stratigraphy of the best-fit model was further established using 16 radiocarbon ages obtained from five boreholes in the estuary. The present approach is particularly suitable for simulating long-term morphological evolution in sheltered estuarine environments where tidally driven vertical aggradation dominates at centennial to millennium timescales. However, the accuracy of simulated sediment surface elevations and consequently the robustness of behaviour-type models based on Geographical Information System platforms can be enhanced by incorporating (i) the impacts of nearshore hydrodynamic processes and episodic flood events in highly energetic channels, and (ii) the impacts of cross-currents in meandering channel sections.

Keywords: Guadiana estuary; Hindcasting; Morphological evolution; Sea-level rise; Behaviour-oriented models

1.0 Introduction

An estuary is a semi-enclosed water body that is associated with a complex mosaic of ecosystems linking terrestrial and aquatic environments, including the subtidal, intertidal, and surrounding terrestrial habitats. These highly complex and diverse systems are sensitive to natural forcing, as generated by sea-level rise, and to human activities such as the development of harbours, shipping channels and recreational facilities (Lanzoni and Seminara, 2002). Estuaries are ephemeral features that during the eustatic sea-level rise of the last 15,000 years progressed along drowned fluvial valleys (Schubel, 1971; Perillo, 1995). Under natural sediment supply conditions, these estuaries have gradually adapted to the prevailing hydrodynamic conditions during the period of sea-level stabilization (Lanzoni and Seminara, 2002). According to Cooper et al. (2012), some evidence suggests that incised valley estuarine systems exhibit an adaptive capacity in response to sea-level rise (e.g. “keep-up” and “catch up” estuaries) while tending towards equilibrium conditions in which the local

sea-level rise is balanced by the sediment accumulation (Stevenson et al., 1986; Nichols, 1989).

The morphological evolution of an estuary is the result of non-linear interactions between water, sedimentary processes, and bathymetry during both fluvial and marine flooding, which occur over a wide range of temporal and spatial scales (Hibma et al., 2004). According to Friedrichs et al. (1990), an increase in sea level in an estuarine system where the banks have curved profiles initially results in channel deepening and the expansion of accommodation space, thereby enhancing ebb and flood asymmetry (i.e., the difference between peak ebb and flood tidal currents). Consequently, more sediment from marine and/or fluvial sources enters the estuary, resulting in an increase in sediment deposition rates and a decrease in depth, thereby reducing the marine influence (Pethick, 1994; Anthony et al., 2002). If the sediment supply is unhindered, this feedback process will lead the estuary to achieve a new equilibrium state. Throughout the Holocene, estuarine systems migrated landwards in response to sea-level rise in a two-stage feedback process (Townend and Pethick, 2002): (1) horizontal retreat of the seaward margins of salt marshes and upper mudflats, and (2) vertical accretion on the newly submerged surfaces because of increased accommodation space. If there is a decrease in sediment supply and/or rapid increase in sea-level rise above the adaptive capacity of the system, the feedback mechanisms may not be sufficient to maintain stable water depths in an estuary. Thus, according to the classification of Cooper et al. (2012), an estuary can turn into a ‘give-up’ estuary from its original behaviour of either a ‘keep-up’ or ‘catch-up’ estuary.

The coastal zone occupies 18% of the world’s land surface and stretches over 842,000 km (Smith, 2005). Coastal plains and lowland river valleys have always been the most populated areas (Wolanski et al., 2004) in which human activities and associated infrastructure have

increased steadily over the last several centuries (McGranahan et al., 2007). Dams that control the world's major rivers have reduced sediment supply to the shoreline by up to 90% (Syvitski et al., 2005), and shorelines have been further impacted by the construction of coastal defences and by land reclamation (Townend and Pethick, 2002).

Global vulnerability analyses by Nicholls et al. (2007) and IPCC (2007) have predicted an increased vulnerability of the coastal zone to sea-level rise, increased storminess, and climate change. Indeed, the assembled records of altimetric data from the TOPEX/Poseidon, Jason-1, and Jason-2 satellite missions indicate that the average rate of sea-level rise during the period 1993–2009 was 3.4 ± 0.4 mm/yr (Nerem et al., 2010), which is double the 1.7 mm/yr rate of the twentieth century.

The cumulative result of human activities and natural pressures is enhanced erosion, habitat loss, and increased flood risk to the coastal environment (Valiela, 2006). A substantial reduction in the amount of sediment supplied to estuaries reduces vertical accretion and decreases their capacity to keep pace with sea-level rise (Ganju and Schoellhamer, 2010). Such constraints on the adaptive capacity of estuaries to sea-level rise will likely provoke a decrease in the area of wetlands and will affect their habitats in the near future. Many estuarine ecosystems have already lost part of their ability to adapt horizontally (Townend and Pethick, 2002) and vertically (Ganju and Schoellhamer, 2010) in response to sea-level rise. To accommodate these trends in coastal planning and territorial management, a better understanding of the long-term behaviour of an estuarine system is required. Adaptation strategies depend on the ability to integrate information about the geomorphology of the system, knowledge of Holocene estuarine evolution, and information about the forcing conditions such as sea-level rise and tidal conditions across a range of spatial and temporal

scales (Townend, 2010). In particular, the early to mid-Holocene may be useful to understanding future sea-level change (PALSEA, 2010) because rates of eustatic sea-level rise during this period were in the order of 6 mm/yr or more (Stanford et al., 2011; Delgado et al., 2012). Such an acceleration in sea-level rise falls well within the range of recent predictions for the latter part of the twenty-first century (Pfeffer et al., 2008). However in contrast to the Holocene, impacts of rapid sea-level rise in the coming decades require consideration of substantial and widespread human intervention in coastal systems.

To complement field investigations that have described geomorphological history and sea-level change over the last 13,000 years in the Guadiana Estuary of southwestern Iberia (Boski et. al., 2008, 2002; Delgado et al., 2012), in the present study we take a formalised yet simple and idealized model approach based on the behaviour (i.e., the morphological evolutionary trends) of that system. The specific objectives of this study are: (*i*) to simulate the sedimentary infilling of the Guadiana Estuary palaeovalley due to eustatic sea-level rise during the Holocene, and (*ii*) to evaluate model outputs against previous geomorphological and post-glacial palaeoenvironmental reconstructions based on facies interpretation and ^{14}C dating. The simulations were performed using the Estuarine Sedimentation Model (ESM), which follows a behaviour-oriented numerical modelling approach (Bruce et al., 2003) that complements process-based modelling (Townend, 2010).

2. Study area

The Guadiana River is 810 km long and traverses extensive rural areas in Spain and Portugal, including the mining areas of the Iberian Pyrite Belt (Delgado et al., 2012). The Guadiana Estuary (Fig. 1) is located along the southern border between Spain and Portugal. It is a narrow, deeply incised (ca. 80 m below present MSL), bedrock-controlled estuary

experiencing the final stages of sediment infilling, which has led to an incipient coastal progradation (Boski et al., 2008). The estuary, which is ca. 50 km long, has a maximum channel width of 550 m and depths ranging between 5 and 17 m (Wolanski et al., 2006). In 2001, the total dammed area in the watershed increased to 89% with the construction of the Alqueva dam (Gonzalez et al., 2007). Because of the consequent shortage of silt supplied by the river, there has been a rapid decrease in the area of estuarine salt marshes (Sampath et al., 2011). In addition, the construction of jetties at the mouth of the Guadiana River in the 1970s has interrupted the dominant eastward-directed longshore drift. This has resulted in a reduction in the amount of marine sediment supplied to the estuary over the last 35 years. The disruptive effects of the jetties are clearly manifested on the Spanish margin of the estuary, where rapid shoreline retreat at an average rate of 3 m/yr occurred between 1996 and 2005, with a recorded maximum retreat of 4.8 m/yr (Sampath, 2008).

Before the construction of the Alqueva dam, the hydrographic regime of the Guadiana River was characterized by low flows in summer and episodic flooding events in winter. The estuary exhibits a semi-diurnal, meso-tidal regime with a mean range of approximately 2.5 m. The mean neap tidal range is 1.22 m and the mean spring tidal range is 2.82 m (Garel et al., 2009), with a maximum spring tidal range of 3.88 m (Sampath et al., 2011). Tidal wave propagation in the estuary generates currents with velocities exceeding 0.5 m/s (Morales, 1997). The waves in this coastal region can be classified as medium- to low-energy waves, and in terms of frequency of occurrence, 49% of the waves represent Atlantic swells and 51% local sea waves. The mean annual offshore significant wave height is about 1 m with an average period of 4.7 s (Costa et al., 2001).

3.0 Methodology

3.1 Estuarine Sedimentation Model (ESM)

Hindcasting the morphological evolution of the Guadiana Estuary during the Holocene was performed using ESM. This GIS raster-based model was initially developed by Stolper (1996) and takes into account three factors: (1) changes in the rate of sea-level rise, (2) elevation-dependent accommodation space available for the deposition of sediment, and (3) the inundation-dependent vertical accretion rate of sediment (Bruce et al., 2003). In the context of large-scale coastal behaviour modelling (decades to millennia), estuarine evolution was simulated using the dominant driving factors, which are relative sea-level change, the rate of sediment supply, and tidal inundation. Although wave and river dynamics may influence sediment dynamics in the outer and inner portions of the estuary, respectively, tidal currents play a dominant role in controlling sediment transport in tidal regimes where the tidal range is greater than 2 m (Lanzoni and Seminara, 2002). Tidal inundation is strongly dependent on palaeovalley morphology, which determines the accommodation space for fluvial and marine sediments.

ESM does not explicitly take into account estuarine physical processes, such as tidal hydrodynamics, channel-shoal sediment exchange, and gravitational circulation. This implies that it is not possible to represent dynamic interactions and feedbacks that promote morphological change, because of the limited understanding/record of such processes over a centennial timescale. To partially overcome such limitations, we opted to represent estuarine sediment deposition processes using the net long-term representative sedimentation rates derived from borehole data analysis. In addition, we incorporated semi-empirical formulations given by Prandle (2009) to derive the relationships between the long-term net accretion rate coefficients and water depth below maximum high tide for defined time

intervals of several centuries (see section 3.2). The long-term net accretion rate coefficients represent the spatial and temporal distributions of sediment accretion below the maximum high-tide level of the estuary. With respect to the energy levels of the studied estuary, the lower Guadiana estuary lies within an environment sheltered by the extensive barrier and salt marsh system and mobile sandbank located close to the river mouth, which significantly attenuate ocean waves entering the estuary. Therefore, the sediment grain size across the lower estuary bed is practically uniform, except for some variation in the intertidal zone (Morales et al., 2006). Thus, according to the established relationship between hydraulic energy and corresponding grain size (Hamilton, 1979), the distribution of energy across the lower Guadiana Estuary may be assumed to be relatively uniform. The near-uniform distribution of sediment accretion rates observed in the sedimentary profiles of several boreholes drilled in the Guadiana Estuary (Boski et al., 2008, 2002) further supports this hypothesis.

3.2 Application of ESM to the Guadiana estuarine system

Following similar approaches in a number of previous estuarine aggradation models (e.g., Allen, 1995; Morris et al., 2002; Kirwan and Murray, 2008) applied to estuarine systems composed of intertidal mudflats and salt marshes, the rate of relative elevation change (dZ/dt) at a given point and over a known period of time can be represented in terms of (Eq. 1): (1) the rate of sea-level rise (dM_{MSL}/dt), (2) mineral sedimentation rate (dS_{Min}/dt) and organic sedimentation rate (dS_{Org}/dt), (3) erosion due to currents (dE/dt), (4) auto-compaction (dP_{Com}/dt), and (5) deep subsidence (dP_{Sub}/dt):

$$\frac{dZ}{dt} = \frac{dS_{Min}}{dt} + \frac{dS_{Org}}{dt} - \frac{dP_{Com}}{dt} - \frac{dM_{MSL}}{dt} - \frac{dP_{Sub}}{dt} - \frac{dE}{dt} \quad (1)$$

In the Guadiana Estuary, deep subsidence has been found to be negligible (Lobo et al., 2003), and because auto-compaction of the accumulated sediments is insignificant as a result of the

low organic content (Boski et al., 2008), it was assumed that shallow compaction is negligible over a centennial timescale. Hence, the determining factors of the model are mineral sedimentation, erosion, and the rate of sea-level rise (Eq. 2):

$$\frac{dZ}{dt} = \frac{dS_{Min}}{dt} - \frac{dM_{MSL}}{dt} - \frac{dE}{dt} \quad (2)$$

The net annual averaged accretion rate ($\Delta S/\Delta t$) at a given initial depth (h) can be derived by integrating mineral deposition and erosion over each tidal cycle over *M* years with *m* tidal cycles, where ρ_{sed} is the dry density of sediment (Eq. 3). Based on the analysis of annual river discharge from 1947 to 2000, we imposed the estimated six-year (i.e., *M* = 6) cyclic fluctuations of average annual river discharge, namely 380, 300, 25, 75, 150, and 175 m^3/s, to determine the long-term net accretion rates. The calculations were computed for each depth with 0.5-m intervals from low-tide level to the maximum depth. This provides variations in net annual average accretion rates from low tide to the maximum depth.

$$\Delta S/\Delta t|_{\text{at a given location}} = \frac{1}{M \times \rho_{Sed}} \sum_{j=1}^{m} \left\{ \int_0^T \left(\frac{dS_{Min}}{dt} - \frac{dE}{dt} \right) dt \right\} \quad (3)$$

Implementation of ESM also requires the long-term net accretion rate coefficients, that is, the long-term net accretion rates relative to the maximum sedimentation rate found within a hypothetical transect from low-tide level to the maximum depth of the estuary (Eq. 4):

$$\text{Long-term net accretion rate coefficient} = \frac{\Delta S/\Delta t|_{\text{at a given location}}}{\Delta S/\Delta t|_{Max}} \quad (4)$$

If a representative value for the maximum annual sedimentation rate (S^{rep}) for a given period in an estuary can be found, the long-term net accretion rate coefficients enable the spatial distribution of net annual sedimentation rates for the given depth range to be calculated (Eq. 5). For simplicity and convenience, we used as S^{rep} the sedimentation rates calculated in

radiocarbon-dated time intervals in six boreholes drilled into the Holocene sedimentary column of the Guadiana estuary. Thus, the net accretion rate at a given depth below the low-tide level can be expressed directly by Eq. 5:

$$\frac{\Delta S_{Net}}{\Delta T} = S^{Rep}\left(\frac{\Delta S/\Delta t|_{\text{at a given location}}}{\Delta S/\Delta t|_{Max}}\right) \quad (5)$$

As given in Equation 6, the net accretion rates above the low tide were derived by incorporating the tidal inundation frequency (Sampath et al., 2011) and the long-term net accretion rate coefficient at the low-tide level (taken from the Portuguese Hydrographic Chart Datum as 2 m below MSL). Consequently, the curves for the long-term net sediment accretion rate coefficients were computed for the entire depth range (i.e., from high-tide level to the maximum depth at 0.5-m intervals) of the estuary for different periods from 11,500 cal. yr BP. The average granulometric sizes of accumulated sediments were assumed to be indicative of the environmental conditions prevailing over specific periods during the Holocene (see section 3.4).

$$\left.\frac{\Delta S_{Net}}{\Delta T}\right|_{\substack{\text{Intertidal}\\ \text{zone}}} = S^{Rep}\left\{\frac{\Delta S/\Delta t|_{@\ z=-2\ m}}{\Delta S/\Delta t|_{Max}}\left[\frac{\text{Tidal Inundation Frequency}|_{@\ z>-2\ m}}{\text{Tidal Inundation Frequency}|_{@\ z=-2\ m}}\right]\right\} \quad (6)$$

Finally, the long-term rate of sediment surface elevation change ($\Delta Z/\Delta T$) at a given point of an estuarine system can be expressed in terms of net sedimentation rate ($\Delta S_{Net}/\Delta T$) and sea-level rise rate ($\Delta H/\Delta T$) (Eq. 7):

$$\frac{\Delta Z}{\Delta T} = \frac{\Delta S_{Net}}{\Delta T} - \frac{\Delta H}{\Delta T} \quad (7)$$

Summarizing the above rationale, our exact input parameters for the ESM model were the long-term net accretion rate coefficients for the depth range, representative sedimentation

rates, and cumulative sea-level rise for the total time period of 11,500 years (and using a five-year time step for the modelling).

3.3 Sediment deposition and erosion over a tidal cycle

The rate of sediment deposition in sub-tidal channels can be approximated by calculating accretion and erosion rates (Equation 3). As the present study is focused on simulating the long-term morphological evolution of estuaries, the re-suspension of sediment due to turbulence can be neglected and therefore the estuary bed can be considered as fully absorptive (Sanford and Halka, 1993). Consequently, the sediment deposition rate (m/s) can be represented in terms of settling velocity (W_s), sediment concentration near the bed (C_b), and the bulk density of sediment (ρ_{sed}) (Prandle, 2009):

$$\frac{dS}{dt} = \frac{W_s C_b}{\rho_{sed}} \quad (8)$$

The settling velocity of fine to medium sand particles ($D_{50} \approx 0.125–0.35$ mm) was estimated in terms of the kinematic viscosity of water, average grain size diameter (D_{50}), and non-dimensional grain diameter (Hallermeier, 1981). The settling velocity of silt to very fine sand fractions ($D_{50} \approx 0.25–0.125$ mm) was derived using the formula of Lane and Prandle (2006) to account for the increase in settling velocity due to the flocculation of particles. Morales (1995) proposed an empirical model for estimating the depth-averaged sediment concentration in the Guadiana estuary in terms of river discharge (m^3/s). The suspended sediment concentration near the bed was related to depth-averaged sediment concentration where sediment deposition occurs via advection and dispersion (Prandle, 2009). The lack of knowledge of river flow rates during the Holocene is also a major constraint. To address this we used the oldest archived data measured in the Guadiana river, available from the Pulo do Lobo gauge station since the 1940s. Although limited in time this record allows us to represent the characteristic torrential river flow regime of the Guadiana river, which we

assume to have been similar over the past millennia. Although we used data and relationships that relate to the recent behaviour of the estuary for hindcasting suspended sediment concentrations in the Guadiana River during the Holocene, these formulae were used because our focus is to conceptualize the problem of the modelling of long-term estuarine morphological evolution. Prandle (2009) showed that time-series of C_b can be related to the depth-averaged sediment concentration in an estuary.

The short-term erosion rate in an estuary can be approximated using the simple formula of Prandle (2004), where γ and f are the sediment erosion coefficient and the bed friction coefficient, respectively:

$$\frac{dE}{dt} = \frac{\gamma f \rho_{w(U_t)^2}}{\rho_{Sed}} \quad (9)$$

The grain density was set to a default value of 2650 kg/m^3, representative of quartz. The expression derived by Jones (1983) was used to estimate the bed friction in terms of bed roughness, which can be related to drag resulting from ripple/dune formations, and the skin friction, which is related to the grain size, D_{50}, of coarse sand for a hydraulically rough flow (Reeve et al., 2004). Values of D_{50} have been given by Morales et al. (2006). As presented by Lane (2004), the main constituents of current speed (U_t) were assumed to be semi-diurnal (M_2) and quarter-diurnal (M_4) tidal currents and residual currents due to river discharge:

$$U_t = U^* \cos(\omega t) - aU^* \cos(2\omega t - \theta) - aU^* \cos\theta \quad (10)$$

where $a=\zeta^*/h$ and θ is the phase angle between tidal elevation and tidal current.

Prandle (2009) simplified the equations for motion at any depth by neglecting convective terms and linearising the frictional terms. Thus, the tidal current amplitude U* was presented for synchronous estuarine condition, where the spatial gradient in tidal elevation amplitude

(ζ^*) is zero and k is a unique wave number for the axial propagation of current and surface elevation:

$$U^* = \zeta^* g \frac{k}{(\omega^2 + F^2)^{0.5}} \quad (11)$$

The linearised dimensionless bed friction coefficient (F) was related to the phase angle (θ) and tidal frequency (ω), and can be estimated using Equation 12, where $\partial h/\partial x$ is the axial bed slope and assumed to be a constant, h is water depth, and g is gravitational acceleration (Prandle 2009).

$$\tan\theta = -\frac{F}{\omega} = \frac{\partial h/\partial x}{0.5hk} \quad (12)$$

where

$$k = \frac{\omega}{\sqrt{0.5hg}} \quad (13)$$

In the Guadiana Estuary, the tidal wave propagates in synchronic mode up to 50 km from the mouth (Morales 1997). This characteristic may be preserved even during spring tides, as the tidal-range attenuation is less than 20 cm per 10 km along the longitudinal axis of the river (Garel et al., 2009). The use of the above assumption can be justified because we consider only the lower Guadiana estuary (11.6 km). The tidal amplitude (ζ^*) was estimated using the amplitudes (ζ_i), angular frequency (ω_i), and phase (ϕ_i) of the five principal constituents (O1, K1, M2, S2, and M4) given by Pinto (2003) for the Guadiana Estuary.

3.4 Hindcasting of sediment infilling

There are two distinct linear relationships for radiocarbon ages versus depths of dated materials from six boreholes in the Guadiana estuary. The first comprehends the period from 13000 cal. yr BP to 7500 cal. yr BP and the second the period since 7500 cal. yr BP to present-day (Boski et al., 2002; 2008; Delgado et al., 2012). This suggests that the sediment accretion is almost linear in those two periods, particularly in the sheltered sections of the

estuary. To determine the grain size of sediments deposited since 11.500 cal. yr BP, an analysis of sediment characteristics from borehole samples was performed. This allowed the definition of 12 granulometrically homogenous time intervals with millennial to centennial time scales, each characterized by virtually constant depositional conditions. The sediment erosion coefficient, γ, is a function of sediment diameter (Lane and Prandle, 2006) and is related to the erodibility of sediment. Two different distributions for γ with depth were assumed while maintaining its average value around 0.0001 $m^{-1}s$, as suggested by Prandle (2004). In this way, variability in grain size across the estuary could be indirectly incorporated into the model. For each distribution of γ, we derived 12 long-term net accretion rate coefficient curves (Fig. 2) corresponding to time periods during which hydrodynamic and environmental conditions were assumed to be uniform throughout the Holocene period.

Four trials were carried out to find the best function for γ and the corresponding set of long-term net accretion rate coefficient curves. The representative sedimentation rates for the first trial were equal to the rate of sea-level rise derived from the analysis of borehole data (Table 1). However, two boreholes are located in a highly sheltered environment and are not, therefore, representative of the lower estuary as a whole. Consequently, trials two to four were performed using stratigraphic data from the remaining four boreholes to find representative sedimentation rates during the Holocene.

Considering specifically the sea-level change since the last glacial maximum (LGM) along the southern Iberia coast, sea-level curves have been presented for coastal areas in the Gulf of Cadiz and in western Portugal (e.g. Dias et al., 2000; Delgado et al., 2012). According to the depth–age diagrams for the Guadiana estuary presented by Boski et al. (2002) and Fletcher et al. (2007), Holocene sedimentation began, respectively, at depths of 42 m and 38 m below present MSL. Recently, Boski et al. (2008), considering the Guadiana and Gilão-Almargem

estuarine systems, placed the beginning of Holocene sedimentation in the southeastern Algarve coast at a depth of 39 m below present MSL. These values are significantly greater than the 30 to 32 m below present MSL extrapolated from the age–depth diagram proposed by Lario et al. (2002) as a synthesis for the Spanish estuaries in the Gulf of Cadiz.

Therefore, considering various estimations of sea level at 11,500 cal. yr BP for the Guadiana estuary, a mean value of 40 m below present MSL was used for simulating the morphological evolution of the Guadiana estuary during the Holocene. In relation to sea-level change since the last glacial maximum (LGM) along the coast of southern Iberia, a sea-level curve has recently been presented for coastal areas in the Gulf of Cadiz and in western Portugal by Delgado et al. (2012). The average rate of sea-level rise proposed for the period 13,000 to 7000 cal. yr BP was estimated at 7.5 mm/yr and the rate for the period since 7500 cal. yr BP until the present was estimated at 1.3 mm/yr. Such a pattern of sea-level rise is consistent throughout the northern Gulf of Cadiz, as evidenced by Zazo et al. (2008), and even along western Iberia Holocene sea-level rise is characterized by such contrasting linear trends of fast increase before and after 7000 cal. yr BP (Vis et al., 2008). For 11,500 cal. yr BP, the error on the position of sea level is approximately ±5 m. This value was estimated from the results of Delgado et al. (2012). The error contains the uncertainties of ^{14}C dating and the uncertainties of past sea-level determination with respect to MSL.

The input and output time-steps were 5 and 10 years, respectively. The simulation of palaeovalley sedimentation from 11,500 cal. yr BP to the present was performed in several blocks with intervals of 100 or 200 years. The final digital elevation model (DEM) of the estuary's bathymetry in each preceding time-step was fed as input into the next step until reaching the present bathymetry. If the simulated elevation values of the DEM corresponding

to the present of a particular trial were comparable to the actual elevation values of the present-day topography, then the corresponding series of bathymetries were considered to be the best possible approximation of the morphological evolution of the estuary for the period since 11,500 cal. yr BP. The corresponding γ and the set of long-term net accretion rate coefficient curves were accordingly considered the best functions for the simulations of long-term sediment infilling, providing a basis for decadal forecasting of the morphological evolution of the estuary during the twenty-first century.

3.5 Digital terrain model of the pre-inundation Guadiana palaeovalley

Exploratory DEMs were created with a suite of the most widely used interpolation methods (Yue et al., 2007; Erdogan, 2009), which are incorporated into the ESRI ArcGIS software used in the present study. Since there is no explicit rule indicating which method is most adequate for a particular surface (Erdogan, 2009), the selection of the interpolation method is more complex, requiring both visual and statistical exploration (Andrews et al., 2002). Methods included TIN (triangulated irregular network with linear interpolation), IDW (inverse distance weighted), Spline and Kriging. ANUDEM, a dedicated interpolation method for creating hydrologically correct DEMs (Hutchinson, 1988, 1989), and implemented in ArcGIS, was also used. As most interpolation methods require input data in the form of individual points, the manually digitized palaeovalley contours were transformed into point features. Each vertex along the contour lines was converted into a point, retaining the corresponding planimetric coordinates and elevation value.

From simple visual observation, the TIN method was excluded for use due to its unrealistic representation of the terrain surface and overall shape unreliability, confirming the general inability of linear interpolation to produce a smooth and natural terrain surface (DeMers,

2002). The remaining interpolation methods were evaluated using cross-validation on a random sample of 10% of the data points (corresponding to 16,112 points). The differences between the interpolated and observed elevation values at each cross-validation point were analysed using standard descriptive statistics for the assessment of DEM accuracy (Fischer and Tate, 2006). The most common statistical descriptor is the root mean square error (RMSE) (Li, 1988; Fisher and Tate, 2006). Two other descriptors suggested by Li (1988), the mean error (ME) and error standard deviation (S), which are often used for a more complete statistical description of DEM interpolation error (Desmet, 1997; Fisher and Tate, 2006), were also calculated. The two extreme values for the difference between the interpolated and observed elevations (positive maximum and negative maximum) were also calculated, indicating the general location of all the other values (Li, 1988).

The results for the descriptive statistics indicated that no method clearly out-performed the others, although the IDW method presented the best results for the extreme values and ANUDEM the best (lowest) values for RMSE and error standard deviation (S). Nevertheless, the results are very similar for the suite of interpolation methods evaluated, with mean errors in the order of a few centimetres and values of RMSE and error standard deviation between 2 and 2.5 m. Thus, ANUDEM was used as the most reasonable interpolation technique for developing the DEM of the Guadiana estuary palaeovalley of 11,500 cal. yr BP (Fig. 3).

4.0 Results

4.1 Morphological evolution of the estuarine palaeovalley during the Holocene

The model-generated DEMs of the present topography in the lower Guadiana Estuary corresponding to each of the four simulation trials are shown in Fig. 4. The reconstructed palaeovalley DEM at 11,500 cal. yr BP (Fig. 4a) and actual present DEM (Fig. 4b) were used

for assessing the simulated results. The first simulation of present-day topography (Fig. 4c) extensively under-predicted the actual topography of the estuary. The only similarity between these two surfaces was in the elevation range from 4 to 5 m. Various important features of the Guadiana estuarine system, including the morphological evolution of the intertidal zone area, the closure of the second mouth of the Guadiana river due to sand infilling, the morphological evolution of the Vila Real St Antonio delta, and the sand-spit developments of Isla Canela and Isla Cristina resulting in the progradation of the Spanish coastline, were not predicted satisfactorily in the first simulation. Even though high sedimentation rates (see Table 1) were used in the second simulation, the simulated topography (Fig. 4d) was still under-predicted and very similar to the results of the first simulation. However, there were some improvements in the upper limits of the intertidal zone compared to the actual elevations, despite a continuing submergence of a large part of the delta located near present-day Vila Real city. The complete closure of the second mouth of the Guadiana River, located near present-day Monte Gordo city, was also not satisfactorily simulated.

The simulated present topography of the estuary obtained in the third simulation (Fig. 4e) shows increased sediment infilling in both the intertidal zone area and the ebb delta close to present-day Vila Real de Santo Antonio city (VRSA). However, this simulation still did not satisfactorily predict the actual morphology of the Guadiana Estuary. This third stimulation presented an equilibrium between the reconstructed Holocene sediment surface topography and simulated topography at a depth of approximately −0.75 m (i.e., the estuary bed at around −0.75 m kept pace with sea-level rise). Spatial analysis shows an equilibrium between actual topography and the Holocene topography in the high-tide region (around +1.6 to + 2 m MSL).

As explained in section 3.4, the results of the fourth simulation correspond to corrected (i.e., forcing equilibrium near the high-tide region) sedimentation rate coefficients compared with the third simulation. This enabled a realistic sediment infilling in both the intertidal zone and part of the main estuarine channel to be achieved (Fig. 4f), and reflected the new relationship between the long-term net accretion rate coefficients and the depth below maximum high tide, leading to a realistic improvement in the simulated shoreface. However, the closure of the second mouth of the Guadiana River and the development of the Isla Canela and Isla Cristina sand-spits were again not adequately predicted. Despite an improvement in the area of the VRSA delta, the evolution of the interface between the estuary and shoreface could not be simulated simply by using this idealized aggradation model. It appears that this highly dynamic boundary follows a complex interplay between tidally driven estuarine vertical aggradation and shoreface processes controlled by both along- and cross-shore sediment drift, resulting in the development and migration of sand spits and subsequent aeolian dune formations.

4.2 Detailed analysis of sediment infilling in the fourth simulation

The fourth simulation was particularly successful in predicting the present-day elevation/morphology of the sheltered environments of the Guadiana estuary. Fig. 5 shows a chronological sequence of sediment infilling along a selected line connecting five boreholes (marked as CM-4, CM-3, CM-1, CM-6 and CM-5 according to their spatial location upstream of the estuary mouth) drilled in the Portuguese margin of the estuary. Locations of five boreholes are also shown in Fig. 4b. The validity of this modelling approach was further tested using nine cross-sections along the main channel, located at distances of 650 m (CM-4), 2100 m, 3300 m (CM-3), 4500 m, 5800 m (CM-1), 7000 m, 8500 m, 9600 m (CM-6), and 10,400 m (CM-5) m from the mouth of the estuary (Fig. 6). Ages obtained from radiocarbon

(^{14}C) analysis corresponding to the five boreholes (Boski et al. 2008, 2002; Delgado et al., 2012), are also plotted on Fig. 6. Each cross-section consists of 14 profiles, corresponding to profiles at 11,500, 11,000, 10,000, 9000, 8000, 7000, 6000, 5000, 4000, 3000, 2000, and 1000 cal. yr BP, and to the simulated and actual profiles for the present-day.

Detailed analysis of sedimentological, mineralogical, paleontological and geochemical data were used to interpret the various sub-environments in the sedimentary columns of the five boreholes, details for which are provided in Boski et al. (2002; 2008) and Delgado et al. (2012). In cross-section 1, borehole CM4 is located approximately 2500 m from the central axis of the estuary channel and on the Monte Gordo dune field (Figs. 1, 6i). Seven sedimentological units can be distinguished in the sedimentary column overlying the Palaeozoic substratum (Boski et al., 2002): (1) fluvial from 31 to 27 m below MSL, (2) salt marsh from 27 to 23 m below MSL, (3) swamp/fluvial wetland from 23 to 20 m below MSL, (4) delta fan from 20 to 14 m below MSL, (5) fluvial river channel from 14 to 11 m below MSL, (6) barrier complex from 11 m below MSL to 3 m above MSL, and (7) dune field from 3 to 5 m above MSL (Fig. 7a). The depths corresponding to ages obtained from borehole CM-4 are discordant with the simulated depths. As this borehole is close to the shoreline, along-shore and cross-shore sediment transportation would be the dominant processes that determined the formation of the barrier complex at least until c. 6437 cal. yr BP. Ages obtained from radiocarbon analysis corresponding to the five boreholes (Boski et al. 2008, 2002; Delgado et al., 2012), are also on Fig. 6, 7, 8 and 9 and fully presented in Table 2. Throughout the text cal. yr BP refer to the median or mid-point date for the two sigma range determined from calibration analysis. For full description of the uncertainty in the radiocarbon ages the reader is referred to Table 2. However, being close to the shoreline, the location of the borehole would have been subjected to episodic extreme events such as storm surges. In such situations, soil layers may not necessarily be in proper chronological sequence

in borehole CM-4, and this may explain why the radiocarbon date of c. 7159 cal. yr BP is found above the radiocarbon date of c. 6437 cal. yr BP. Finally, aeolian processes would be the dominant controlling factors of sediment infilling. The discrepancy in the chronology between the measured and modelled infilling is because the above-mentioned processes were not included in the ESM model.

In cross-section 3, borehole CM-3 was located close to the river mouth at 11,500 cal. yr BP in the Portuguese margin and approximately 1300 m from the central axis along the estuary channel. The borehole is within the salt marsh affected sporadically by spring tides, and four units of sedimentological facies lying over the Palaeozoic substratum reached at a depth of 35 m can be identified (Boski et al., 2002): (1) fluvial river channel from 35 to 29.8 m below MSL, (2) upper salt marsh from 29.8 to 15.5 m below MSL, (3) lower salt marsh from 15.5 to 1.8 m below MSL, and (4) present anthropic soil from 1.8 m below MSL to 1.0 m above MSL (Fig. 7b). The simulated and actual present topographies are compatible with each other in the location of borehole CM-3 in cross-section 3. Infilling depths for radiocarbon ages of c. 3598, 7594, and 7936 cal. yr BP are comparable with corresponding simulated depths whereas the depth value for c. 10738 cal. yr BP shows a shift to a depth corresponding to that for c. 9815 cal. yr BP (Fig. 6iii).

Borehole CM-1 is located in cross-section 5 and is situated in the tidally active salt marsh near Castro Marim. According to Boski et al. (2002), five lithological units can be distinguished above the bedrock at a depth of 41 m below MSL, namely: (1) fluvial river channel from 41 to38 m below MSL, (2) upper salt marsh from 38 to 19 m below MSL, (3) tidal flats from 19 to 18 m below MSL, (4) upper salt marsh from 18 to 15 m below MSL, and (5) lower salt marsh from 15 to 1 m below MSL. In addition, there is a 1-m-deep anthropic soil layer up to the surface (Fig. 7c). The simulated and observed present

topographies are compatible with each other in the location of borehole CM-1 (Fig. 6vi). The depth values for c. 10,765, 9420, 8848, and 3210 cal. yr BP are comparable with those of the simulated depths, whereas the depth values at c. 7175, 7155, and 5837 cal. yr BP cannot be matched to corresponding simulated depth values. The continuity of the upper salt marshes has been disturbed by the deposition of a ~1-m-thick layer of medium sand, forming a tidal flat for a short period.

In cross-section 8 (Fig. 6viii), borehole CM-6 is located on mudflats in the Spanish margin and is 500 m from the central axis (near the Beliche bend of the Guadiana River). Sedimentary sequences of borehole CM-6 have accreted on top of a coarse to very coarse basal gravel layer (Fig. 8a) that was deposited by the Guadiana River during a past marine lowstand (Delgado et al., 2012). Although the simulated and actual present topographies are compatible with each other, only two depth values (at c. 897 and 1155 cal. yr BP) approximate the corresponding simulated values, whereas depth values at c. 742, 6917, and 7612 cal. yr BP are not comparable to their respective simulated depths. The sedimentary facies in borehole CM-6 from 11,500 cal. yr BP to the present represent a transition from fluvial river channel to salt marsh and then to a mudflat (Delgado et al., 2012). According to the observed sediment granulometry from c. 6917 cal. yr BP to the present, at least three episodic extreme events may have occurred during this period, and may explain the discordance of the depths at c. 7612 and 6917 cal. yr BP with the corresponding simulated values. However, there is an additional process around bends in rivers and channels that should be considered. Cross-currents in channels produce higher elevations near the outside curve of the channel and low flow near the inside curve of the channel. In such a situation, eddy currents would occur, resulting in a loss of energy. As a result, there would be an increase in sediment deposition near the inside curve of the channel. However, increase of inundation hydroperiod due to elevated water depths near the outside curve of the channel

results in increasing current velocity and erosion. This process may explain why the path of the Guadiana estuary profile migrated towards the Portuguese margin while enhancing fluvial sediment deposition in the inner region. Because such processes were not included in the ESM, we cannot expect complete agreement between the simulated and observed depositional facies.

In section 9, the most landward borehole, CM-5, is located near the Beliche Rivulet in the Portuguese margin. As in borehole CM-6, sedimentary sequences have accumulated on top of a coarse to very coarse basal gravel layer, which was deposited by the Guadiana River during a past marine lowstand (Delgado et al., 2012). According to Boski et al. (2008), depositional facies can be identified, related to (1) a transition from fluvial river channel to estuarine channel from 47.1 to 39.3 m below MSL, (2) salt marsh from 39.3 to 23 m below MSL, (3) mudflat from 23 to 2.7 m below MSL, (4) salt marsh from 2.7 m below MSL to 0.5 above MSL, and (5) a 1-m-thick layer of anthropic soil from 0.5 m above MSL to the present surface (Fig. 8b). Depth values for the ^{14}C ages can be compared to the corresponding simulated depths. The successful comparability in the present case may be attributed to the sheltered nature of the location of borehole CM-5. In summary, infilling depths related to 16 age determinations are approximately compatible with the corresponding depths simulated using the ESM model, whereas 10 are not. A comparison between the depths and radiocarbon ages of 26 samples and the modelled depths for the same temporal waypoints (Fig. 9) demonstrates a very good agreement, with statistical significant correlation at the 0.01 confidence level and a R^2 value of 0.722. This indicates a high accuracy, particularly considering the uncertainties in modelling sedimentation on millennial time scales.

On the whole, the Portuguese and Spanish margins in cross-section 1 of the simulated profile have to be infilled with sediment by approximately 2.4 and 7 m, respectively, to be compatible with the actual present profile. However, the simulated sub-tidal region of the estuary was overfilled by about 3.7 m of sediment. There are similar inaccuracies in cross-sections 2, 3 and 4. The errors may have occurred as a result of the formation of sand dunes near to the coastline. However, the average errors in cross-sections 5, 6 and 7 are less than 1 m. Furthermore, the meandering of the main channel of the estuary may have contributed to inaccuracies in the sub-tidal regions of cross-sections 4 to 7. On average, the modelled present-day profiles of cross-sections 8 and 9 have to be infilled with approximately 2.5 m of sediment to make them compatible with the corresponding actual present-day profiles. However, the incompatibilities are seen mainly for the higher elevations, where there is no influence of tides or waves. Therefore, it would appear that the errors are associated mainly with the initial inaccuracies involved in reconstructing the palaeovalley of 11,500 cal. yr BP. The other possible source of error in the sub-tidal region of the estuary is channel dredging for navigation purposes or channel scour/avulsion processes that cannot be captured in the modelling.

5.0 Discussion

5.1 Accuracy of the model results

Stratigraphic sequences provide empirical records of global environmental conditions and changes (Burke et al., 1990). Studies of the magnitude and frequency of past global changes can be used to understand historical trends and to predict near-future conditions (Blum and Törnqvist, 2000). In this context, an understanding of past and present trends in sea-level rise is particularly important for simulating the morphological evolution of coastal areas using a behaviour-oriented modelling approach. For the present study, the definition of the mean sea-

level for the start of the Holocene, considering that this occurred at 11,500 cal. yr BP (Bjorck et al., 1998), was based on published regional relative sea-level curves along with published information on discrete relative sea levels and sediment accumulation rates along the Cadiz Gulf during the Late Pleistocene to Holocene transition.

The simplest assessment of the model results presented here may be achieved by comparing the simulated and actual present-day topographies of the Guadiana Estuary (Fig. 10). If the actual and simulated elevations are the same, then the gradient of the corresponding linear regression plots is equal to 1 and the simulation is 100% accurate. However, the direct comparison of two DEMs is compromised by human activities of the past centuries, which has significantly altered local physiography. Since bathymetric data do not cover a period of more than a century, and given that such data may contain signatures of past human activity, we may not be able to achieve perfect validation of the model results. In coastal settings, determining the chronology with good temporal resolution for palaeoenvironmental changes is highly dependent on availability of organic material for ^{14}C dating (Kortekaas, 2007). In the present study, the determination of ages at different depths of the estuarine system was based on several samples suitable for radiocarbon dating. However, the poor temporal resolution of ^{14}C-dated sediment samples constrains the validation of the morphological evolution model.

Still, according to the best-fit solution obtained from the four iterations, the linear regression gradients of actual elevation versus simulated elevation along the cross-sections in sheltered environments of the estuary (cross-sections 4 to 9) are greater than 0.67, whereas the gradients of the cross-sections located near the shoreface (cross-sections 1 to 3) are less than 0.50. In addition, the R^2 values for plots corresponding to cross-sections 4 to 9 are greater than 0.82. That is, the model results corresponding to sheltered environments of the estuary

are very much within the acceptable limits of accuracy given that the simulations are based on a millennial time scale.

The simplicity of the regression-based assessment means that it does not provide a complete picture of the accuracy of the adopted modelling technique. The RMSE of simulated water depths (Table 3) was therefore used as a more robust estimator of accuracy. For that purpose, we converted the final raster DEMs of the four simulations into point data sets (bathymetry), using ArcGIS tools. Each data set was divided into four topographic sections (Fig. 11) and compared with observed present-day (year 2000) morphology. On the whole, there was a significant reduction in the RMSE for all four topographic sections through the successive simulations numbered 1 to 4, except in topographic section 4 of the fourth simulation. For simulations 3 and 4, there was a slight increase in the RMSE in topographic section 4 compared to that in topographic section 3. Nevertheless, it is fair to conclude that the RMSE generally decreases with distance from the mouth of the estuary.

Although the total RMSE of ±4.8 m in the fourth simulation seems high, it is important to consider that the possible errors in determining the MSL at 11,500 cal. yr BP were in the order of ±5 m (Delgado et al., 2012). The effect on the accuracy of the DEM of the input palaeovalley at 11,500 cal. yr BP caused by interpolation errors can also contribute to the overall accuracy of the model. As proposed by Fisher and Tate (2006) and Li (1988), both the RMSE and error standard deviation were used for determining the accuracy of the DEM of the 11,500 cal. yr BP palaeovalley. Values of both these descriptors lay in the range of 2–2.5 m. The total RMSE in the simulated elevations is, therefore, within this initial error margin.

Further improvement in the assessment of the quality of modelled palaeotopography was achieved by computing the average error in accretion height (AEAH) of each simulated DEM relative to the average actual accretion height for the whole estuarine system (Table 3):

$$AEAH = \frac{\frac{1}{n}\sum_{i}^{n} Error\ in\ simulated\ accretion\ height}{\frac{1}{n}\sum_{i}^{n} Actual\ accretion\ height} \quad (14)$$

where *i* is the particular cell identification and *n* is the number cells in each DEM.

The AEAH of the fourth simulated DEM relative to the actual values was 27.5%, an acceptable figure considering the millennial timescale of simulations. Consequently, we can conclude that the behaviour-oriented approach presented here is satisfactory for simulating the morphological evolution of estuarine systems over centennial to millennial timescales.

5.2 Limitations of the modelling approach

The uncertainties in hindcasting the morphological evolution of the Guadiana Estuary arise from the following causes: (1) a high degree of generalization/simplification of the infilling processes; (2) a lack of comprehensive data to characterise the physical environment of the estuary over the considered period, such as tidal pattern or river discharge (the deduced probable cyclic fluctuations of the average annual river were considered); (3) the bias caused by the antecedent topography. Analysis of global long-term tide gauge datasets obtained under the present rise sea-level conditions (Woodworth, 2010) suggests that there may be feedback effects on regional tidal dynamics (Ward et al., 2012; Pelling et al., 2013). These are likely to modify tidal regimes and tidal ranges along most coastal environments. Absence of reliable data to estimate tidal range variability in the Guadiana estuary during the Holocene transgression, along with the impossibility to explicitly model hydrodynamics and sediment transport in a behaviour-oriented modelling approach, implies that modelling was performed considering always conditions equal to the contemporary tidal regime. Furthermore, the

evolution of bathymetry in an estuary is sensitive to bed friction (*f*) and to sediment erosion coefficient (γ) (Lane, 2004; Lane and Prandle 2006). The approach that we used to develop relationships between non-dimensional net accretion and depth in the sub-tidal channel are dependent on *f* and γ, whose values along the Holocene are also unknown. To a certain extent, the trial and error approach followed in the four simulations allowed the uncertainties in these parameters to be overcome.

The presented model-based reconstruction relied on the assumption of continuous sedimentation, that is, without periods of non-deposition or erosion that would otherwise reduce the time and space preserved in a sediment column (Sommerfield, 2006). In shallow-marine settings such as estuarine systems, accumulation rates correlate inversely with the time span over which they are averaged, that is, averaging over longer periods typically results in lower accumulation rates (Sadler, 1999, 1981). Sediment accretion rate depends on the inundation hydroperiod (Cahoon and Reed, 1995). When sediment accretes with time, the inundation hydroperiod decreases, so that less sediment deposits leading to a reduction of accretion rate (Fagherazzi, et al., 2007). This suggests that there is a complex non-linear feedback between sediment infilling and inundation hydroperiod in estuarine systems. In addition, the intense physical and biological reworking of the topmost sediment layer in shallow-estuarine settings filters out low-magnitude events and further increases the incompleteness of the sedimentary record (Crowley, 1984). Therefore, the stratigraphic record should be seen as only a partial record of depositional events (Sommerfield, 2006),

and the present model will depend ultimately on the accuracy of long-term representative sedimentation rates derived from borehole data.

The under-prediction of the morphological evolution of the shoreface, in particular the progradation of the coastline of the eastern margin of the estuary, is a salient feature of all four simulations. The shoreface is a highly dynamic zone where waves, currents, tides, cross-shore and longshore sediment transport, local topography and composition of the seabed are interdependent and occur through complex feedback loops (Dronkers, 2005). Likewise, tidal inlets and their associated features, as ebb and flood deltas, add further layers of complexity for modelling entire coastal systems. They act as sources of sediment supply to the coast but with a significant temporal variability, dictated by river discharge (Garel et al., 2014). A complex nearshore sand rotation mechanism proposed by Garel et al. (2014) for the Guadiana estuary, involving feedbacks between sand banks and river flow, which were profoundly altered during cyclic flash-flood events, resulting in migration of sand banks to the eastern margin and subsequent welding to the coastline. This process, conceptualized by Garel et al. (2014) and based on the ebb-tidal delta breaching model by FitzGerald et al. (2000), may have taken place over several millennia on the lower Guadiana estuary, resulting in the progradation of the eastern margin. Such a combination of wave, tide and fluvial dynamics promotes highly nonlinear processes that, given the lack of knowledge of small-scale residual effects on defining the long-term behaviour, significantly hinders their inclusion in millennia scale predictions (Stive et al., 1995). Therefore, given the averaged nature of behaviour-oriented modelling, similar rates of sedimentation (S^{rep}) were considered for the inner estuary and the eastern margin, recognizing that this is a clear limitation of this approach.

In comparison to the projections of coastal evolution in the lower estuary presented by Morales (1997), the under-prediction of simulations seems to embrace the period from 3000 years BP to the present. Even though the projections of Morales (1997) were based on very limited archaeological data from Ojeda (1988), it seems that the transverse growth of the Monte Gordo beach spit took place on the Portuguese margin synchronously with progradation of the Spanish margin due to new barrier islands forming from active sand bars. As sea-level stabilized during the mid-Holocene, sand bodies located west of the present Monte Gordo beach would have migrated eastwards, causing the closure of the secondary river mouth. There is also evidence for rapid hillslope erosion in particular from 3000 to 300 yrs BP, which is considered to relate to pre-Roman, Roman, Moorish and early Portuguese phases of settlement and clearance for agriculture and forestry resulting valley floor deposition and estuary siltation (Plater and Kirby 2006). Therefore, the abundance of sediment in the late Holocene would have enhanced progradation of both western and eastern margins of the Guadiana estuary. Subsequent aeolian sand deposition would have enhanced the morphological evolution of the coastline. As the ESM model cannot simulate these dynamic and stochastic processes on the shoreface, increased sediment infilling and subsequent closure of the second mouth of the Guadiana River (near present-day Monte Gordo), along with progradation of the eastern margin, could not be simulated satisfactorily using the present approach. Therefore, it appears that the ESM is more suited for simulating vertical aggradation processes in sheltered environments of an estuarine system rather than for simulating the lateral movements of sand bodies. A better understanding of the changes in sea-level rise and sediment supply throughout the Holocene is a pre-requisite for long-term modelling of sediment infilling in estuarine systems.

5.3 Suggestions to improve the model approach

There is still room for further improvement of the approach presented. For instance, if a behaviour modelling approach used for simulating the evolution of the shoreface (e.g. Storms et al., 2002) could be incorporated with the present approach of simulating the sheltered environments of an estuary, it would be possible to develop a more generalized application. Incorporating non-linear sediment accumulation rates at least in the shoreface environment would also enhance the accuracy of the simulations. Furthermore, the temporal resolution limitation of dating samples based on ^{14}C could be overcome by optically stimulated luminescence (OSL) as a mean of determining burial ages for sediments (Jacobs, 2010). Considering that suitable material such as sand or silt-sized grains of quartz and feldspar is usually available throughout the site, OSL dating technique could be used to improve the chronological sequence of the sedimentary infilling of the Guadiana estuary with higher temporal resolution since 11500 cal. yr BP.

Particle size data can be used to overcome the lack of comprehensive information to characterise the physical environment of the estuary over the study period. For instance, particle size data can be used as a proxy to represent the changing hydrodynamics, different modes of sediment transport and deposition of back-barrier systems including tidal marshes, and open estuaries (Clarke et al., 2014). According to these authors, such data may be used to explain mesoscale system behaviour at sub-annual resolution over multiple years, and then sub-annual and multi-annual fluctuations in these environmental settings may be superimposed on a longer-term quasi-stable regime. A better understanding of the long-term estuarine evolution can thus be achieved and incompleteness of stratigraphic data due to partial recording of depositional events, as described by Sommerfield (2006), can be avoided to a certain extent.

The formation of sand bars, the closure of inlets or a river mouth due to excess sand infilling, and the formation of aeolian dunes by wind are examples of complex behaviours of estuarine systems. However, further studies may include and help to understand the long-term behaviour of such coastal features and processes in numerical models envisaged in the present study.

Conclusions

To improve the current understanding of the response of estuarine systems to natural forcing, we simulated the morphological evolution of the Guadiana Estuary due to eustatic sea-level rise during the Holocene. The long-term modelling of the morphological evolution in the estuary complemented previous reconstructions, based on interpretations of the experimental data. Simulations were performed using a behaviour-oriented modelling approach for a time frame established based on 26 radiocarbon age determinations. Six out of nine obtained topographic surface profiles closely matched the actual topographic profiles. The simulations proved to be realistic when applied to the sheltered environments of the estuary, for which the vertical aggradation of sediment is the dominant component of the infilling process.

The best model-based reconstruction of present-day morphology obtained in four different simulations had a total root mean square error of ±4.8 m. This error is comparable with that associated with the estimated mean sea level at 11,500 cal. yr BP and with uncertainties in recreating the palaeovalley surface at 11,500 cal. yr BP. The average error in simulating the elevation of the accreted sediment surface relative to the actual average accretion height was 27.5%, and is considered as acceptable for the millennial timescale adopted. The behaviour-oriented approach that was followed in this study appears to be a useful tool for simulating the morphological evolution of an estuarine system during the period of postglacial sea-level

rise. It seems particularly suited to the more sheltered environments of an estuarine system where vertical aggradation dominates the sedimentary infilling of the palaeovalley.

Acknowledgments: The first author acknowledges FCT for granting a scholarship (SFRH/BD/70747/2010) to carry out this work as part of his PhD research. Carlos Loureiro participation is supported by FCT (grant SFRH/BPD/85335/2012). The authors acknowledge David Stolper, Vivira Cadungog, Peter Cowell and Eleanor Bruce, School of Geosciences, University of Sydney, and the Sydney Olympic Park Authority, for the development of and access to the ESM. The comments of two anonymous reviewers and the editor, Andrew Plater, have helped to significantly improve an earlier version of the manuscript.

Captions of Figures and Tables

Figure 1: Location of the lower Guadiana Estuary.

Figure 2: Long-term net accretion rate coefficients as a function of depth of the Guadiana Estuary, where (a) and (b) represent two different distributions of sediment erosion coefficients (γ) with depth, and (c) represents the distribution of γ with depth as in the case of (b) but with an additional proportion of net accretion observed at −0.75 m, which results in an equilibrium depth, compared with the observed equilibrium depth, of +2.0 m.

Figure 3: Three-dimensional view of the reconstructed palaeovalley of the lower Guadiana Estuary at 11,500 cal. yr BP.

Figure 4: Comparison of palaeovalley simulation results corresponding to 0 cal. yr BP with the present-day bathymetry derived from topo-bathymetric surveying in 2000 AD: (a) the palaeovalley of 11,500 cal. yr BP; (b) present-day bathymetry; (c), (d), (e), and (f) simulated present-day bathymetry under simulation runs 1, 2, 3, and 4, respectively.

Figure 5: Three-dimensional sketch of sediment infilling over the Guadiana estuary palaeovalley from 11,500 cal. yr BP to the present (fourth simulation).

Figure 6: Simulated curves of sediment infilling in the Guadiana estuary from 11,500 cal. yr BP to the present and comparison with actual present-day cross-sections.

Figure 7. Lithostratigraphic sequences of boreholes a) CM-4 (Section 1); b) CM-3 (Section 3); and c) CM-1 (Section 5), showing sedimentary units and comparison of depths for ages obtained from radiocarbon (^{14}C) analysis and model simulations (Adapted from Boski et al., 2002).

Figure 8. Lithostratigraphic sequences of boreholes (a) CM-6 (Section 8); and (b) CM-5 (Section 9), showing sedimentary units and comparison of depths for ages obtained from radiocarbon (^{14}C) analysis and model simulations (Adapted from Delgado et al., 2012).

Figure 9: Radiocarbon ages of sampled material from the five boreholes in the Guadiana estuary and the equivalent modelled age for the same depths obtained from the simulation of the sediment infilling of the Guadiana estuary.

Figure 10: Comparison of simulated and actual (observed) elevations for nine cross-sections along the Guadiana estuary for the present-day. The line y = x represents the ideal line for 100% accuracy between simulated and observed elevations.

Figure 11: Sections of the Guadiana estuarine system used for analysing errors on simulated bathymetries.

Table 1: Input data used to model Holocene sediment infilling in the Guadiana Estuary.

Table 2: Summary information for ^{14}C age determinations showing conventional age, δ13C‰, 2 σ range and indicative ages used in the text and Fig. 6, 7, 8 and 9.

Table 3: Comparison of root mean square errors on simulated water depths and corresponding actual depths and average errors on simulated accretion heights relative to those of actual accretion heights of the Guadiana estuarine system from 11,500 cal. yr BP to the present.

References

1. Allen, J.R.L., 1995. Salt marsh growth and Flandrian sea level: implication of a simulation model for Flandrian coastal stratigraphy and peat-based sea-level curves. Sedimentary Geology. 100, 21–45.

2. Andrews, B.D., Gares, P.A., Colby, J.D., 2002. Techniques for GIS modeling of coastal dunes. Geomorphology. 48, 289–308.

3. Anthony, E.J., Oye´de´, L.M., Lang, J.G., 2002. Sedimentation in a fluvially infilling, barrierbound estuary on a wave-dominated, microtidal coast: the Oue´me´ river estuary, Benin, West Africa. Sedimentology. 49, 1095–1112.

4. Bjorck, S., Walker, M.J.C., Cwynar, L.C., Johnsen, S., Knudsen, K., Lowe, J.J., Wohlfarth, B., Intimate Members, 1998. The Holocene transgression into the estuarine central basin of the Odiel River mouth (Cadiz gulf, SW, Spain): lithology and faunal assemblages. Journal of Quaternary Science. 13 (4), 283–292.

5. Blum, M.D., Törnqvist, T.E., 2000. Fluvial responses to climate and sea-level change: a review and look forward. Sedimentology. 47 (Supplement 1), 2–48.

6. Boski, T., Moura, D., Veiga-Pires, C., Camacho, S., Duarte, D., Scott, D.B., Fernandes S.G., 2002. Postglacial sea-level rise and sedimentary response in the Guadiana Estuary, Portugal/Spain border. Sedimentary Geology. 150, 103–122.

7. Boski, T., Camacho, S., Moura, D., Fletcher, W., Wilamowski, A., Veiga-Pires, C., Correia, V., Loureiro, C., Santana, P., 2008. Chronology of post-glacial sea-level rise in two estuaries of the Algarve coast, S. Portugal. Estuarine, Coastal and Shelf Science. 77, 230–244.

8. Bruce, E., Cowell, P., Stolper, D., 2003. Development of a GIS-based estuarine sedimentation model. In: Woodruffe, C.D., Furness, F.A. (Eds.), Coastal GIS 2003 – Wollongong University, Australia, papers on Maritime Policy 14. pp. 271–285.

9. Burke, K., Francis, P., Wells, G., 1990. Importance of the geological record in understanding global change. Palaeogeography, Palaeoclimatology, Palaeoecology. Global and Planetary Change. 89, 193–204.

10. Cahoon, D.R, Reed, D.J., 1995. Relationships among marsh surface topography, hydroperiod, and soil accretion in a deteriorating Louisiana marsh. Journal of Coastal Research. 11(2), 357–369.

11. Clarke, D.W., Boyle, J.F., Chiverrell, R.C., Lario, J., Plater, A.J., 2014. Sediment record of barrier estuary behaviour at the mesoscale: Interpreting high-resolution particle size analysis. Geomorphology. 221, 51– 68.

12. Cooper, J.A.G., Green A.N., Wright, C.I., 2012. Evolution of an incised valley coastal plain estuary under low sediment supply: a 'give-up' estuary. Sedimentology. 59, 899–916. doi: 10.1111/j.1365-3091.2011.01284.x

13. Costa, M., Silva, R., Vitorino, J., 2001. Contribuição para o estudo do clima de agitação maritime na costa portuguesa. 2as Jornadas de Engenharia Costeira e Portuária. Aveiro, Portugal. AIPCN, 20 p. (in CD-ROM).

14. Crowley, K.D., 1984. Filtering of depositional events and the completeness of sedimentary sequences. Journal of Sedimentary Petrology. 54, 127–136.

15. Delgado, J., Boski, T., Nieto, J.M., Pereira, L., Moura, D., Gomes, A., Sousa, C., García-Tenorio, R., 2012. Sea-level rise and anthropogenic activities recorded in the

late Pleistocene/Holocene sedimentary infill of the Guadiana Estuary (SW Iberia). Quaternary Science Reviews. 33, 121–141. DOI: 10.1016/j.quascirev.2011.12.002.

16. DeMers, M., 1997. Fundamentals of Geographic Systems. Wiley, New York, pp. 486.

17. Desmet, P.J.J., 1997. Effects of interpolation errors on the analysis of DEM's. Earth Surface Processes and Landforms. 22, 563– 580.

18. Dias, J. M. A., Boski, T., Rodrigues, A., Magalhães, F., 2000. Coastline evolution in Portugal since the Last Glacial Maximum until present – a synthesis. Marine Geolog. 170, 177–186.

19. Dronkers, J., 2005. Dynamics of coastal systems. Advanced Series on Ocean Engineering, 25. World Scientific Publishing, Singapore. p 519.

20. Erdogan, S., 2009. A comparison of interpolation methods for producing digital elevation models at the field scale. Earth Surface Processes Landforms. 34, 366–376. DOI: 10.1002/esp.1731

21. Fagherazzi, S., Palermo, C., Rulli, M.C., Carniello, L., Defina A., 2007. Wind waves in shallow microtidal basins and the dynamic equilibrium of tidal flats, J. Geophys. Res., 112, F02024, doi:10.1029/2006JF000572.

22. Fisher, P.F., Tate, N.J., 2006. Causes and consequences of error in digital elevation models. Progress in Physical Geography. 30(4), 467–489.

23. FitzGerald, D.M., Kraus, N.C., Hands, E.B., 2000. Natural mechanisms of sediment bypassing at tidal inlets. US Army Corps of Engineers. P 11.

24. Fletcher, W.J., Boski, T., Moura, D., 2007. Palynological evidence for environmental and climatic changes in the lower Guadiana valley (Portugal) during the last 13,000 years. The Holocene. 17, 479–492.

25. Friedrichs, C.T., Aubrey, D.G. and Speer, P.K., 1990. Impacts of relative sea-level rise on evolution of shallow estuaries. In: Cheng, R.T. (Ed), Residual Currents and Long-term Transport. Coastal and Estuarine Studies, Springer, New York, pp. 106–122.

26. Ganju, N.K., Schoellhamer, D.H., 2010. Decadal-timescale estuarine geomorphic change under future scenarios of climate and sediment supply. Estuaries and Coasts 33. 15–29.

27. Garel, E., Sousa, C., Ferreira, Ó. Morales, J.A., 2014. Decadal morphological response of an ebb-tidal delta and down-drift beach to artificial breaching and inlet stabilisation. Geomorphology. 216, 13–25.

28. Garel, E., Pinto, L., Santos, A., Ferreira, ó., 2009. Tidal and river discharge forcing upon water and sediment circulation at a rock-bound estuary (Guadiana Estuary, Portugal). Estuarine, Coastal and Shelf Science. 84, 269–281. DOI 10.1016/j.ecss.2009.07.002.

29. Gonzalez, R., Araújo, M.F., Burdloff, D., Cacha˜o, M., Cascalho, J., Corredeira, C., 2007. Sediment and pollutant transport in the Northern Gulf of Cadiz: a multi-proxy approach. Journal of Marine Systems. 68, 1–23.

30. Hallermeier, R.J., 1981. Terminal velocity of commonly occurring sand grains. Sedimentology. 28, 859–865.

31. Hamilton, D., 1979. The high energy, sand and mud regime of the Severn Estuary, south-west Britain. In: Severn R.T, Dineley, D., Hawker L.E. (Eds.), Tidal Power and Estuary Management. Colston Papers No. 30, Scientechnica, Bristol, pp. 162–172.

32. Hibma, A., Stive, M.J.F., Wang, Z.B., 2004. Estuarine morphodynamics. Coastal Engineering. 51, 765–778.

33. Hutchinson, M.F., 1988. Calculation of hydrologically sound digital elevation models. Proceedings of the Third International Symposium on Spatial Data Handling, August 17–19, Sydney. International Geographical Union, Columbus, Ohio, pp. 117–133.

34. Hutchinson, M.F. 1989. A new method for gridding elevation and streamline data with automatic removal of pits. Journal of Hydrology. 106, 211–232.

35. IPCC 2007. Climate Change 2007: The Physical Science Basis. Contribution of Working Group I to the Fourth Assessment Report of the Intergovernmental Panel on Climate Change, In: Solomon, S., Qin, D., Manning, M., Chen, Z., Marquis, M.,

Averyt, K.B., Tignor, M., Miller, H.L. (Eds.), Cambridge University Press, Cambridge, United Kingdom and New York, NY, USA.

36. Jacobs, Z., 2010. An OSL chronology for the sedimentary deposits from Pinnacle Point Cave 13Bda punctuated presence. J. Hum. Evol. 59 (3-4), 289 – 305.

37. Johns, B., 1983: Turbulence modelling beneath waves over beaches. In: Johns, B. (Ed.), Physical Oceanography of Coastal and Shelf Seas. Elsevier Oceanography Series. 35, 111–133.

38. Kirwan, M.L., Murray, A.B., 2008. Ecological and morphological response of brackish tidal marshland to the next century of sea level rise, Westham Island, British Columbia. Global and Planetary Change. 60, 471–486.

39. Kortekaas, M., Murray, A.S., Bjo¨rck, S., Sandgren, P., 2007. OSL chronology for a sediment core from the southern Baltic Sea: a complete sedimentation record since deglaciation. *Quat. Geochronology. 2*, 95–101.

40. Lane, A., Prandle, D., 2006. Random-walk particle modelling for estimating bathymetric evolution of an estuary. Estuarine, Coastal and Shelf Science, 68, 1–2. 175–187, doi:10.1016/j.ecss.2006.01.016.

41. Lane, A., 2004. Bathymetric evolution of the Mersey Estuary, UK, 1906–1997: causes and effects. Estuarine, Coastal and Shelf Science. 59 (2), 249–263. doi:10.1016/j.ecss.2003.09.003.

42. Lanzoni S., Seminara G., 2002. Long term evolution and morphodynamic equilibrium of tidal channels. Journal of Geophysical Research. 107 (C1), 1–13. DOI:10.1029/2000JC000468.

43. Lario, J., Zazo, C., Goy, J.L., Dabrio, C.J., Borja, F., Silva, P.G., Sierro, F., Gonz!alez, A., Soler, V., Yll, E., 2002. Changes in sedimentation trends in SW Iberia Holocene estuaries (Spain). Quaternary International. 93–94. 171–176.

44. Li, Z., 1988. On the measure of digital terrain model accuracy. Photogrammetric Record. 12 (72), 873–877.

45. Lobo, F.J., Dias, J.M.A., González, R., Hernández-Molina, F.J., Morales, J.A., Díaz del Río, V., 2003. High-resolution seismic stratigraphy of a narrow, bedrock-controlled estuary: the Guadiana estuarine system, SW Iberia. Journal of Sedimentary Research. 73, 973–86.

46. McGranahan, G., Balk, D., Anderson, B., 2007. The rising tide: assessing the risks of climate change and human settlements in low elevation coastal zones. Environment and Urbanisation.19 (1), 17–37.

47. Morales, J.A., 1995. Sedimentologia del estuario del Rio Guadiana (S.W. Espanã–Portugal), Servicio de Publicaciones, Huelva University; 1–322.

48. Morales, J.A., 1997. Evolution and facies architecture of the mesotidal Guadiana River delta (S.W. Spain–Portugal). Marine Geology. 138, 127–148.

49. Morales, J.A., Delgado, I., Gutierrez-Mas, J.M., 2006. Sedimentary characterization of bed types along the Guadiana Estuary (SW Europe) before the construction of the Alqueva dam. Estuarine, Coastal and Shelf Science. 70, 117–131.

50. Morris, J.T., Sundareshwar, P.V., Nietch, C.T., 2002. Responses of coastal wetlands to rising sea level. Ecology. 83, 2869–2877.

51. Nerem, R. S., Chambers, D., Choe, C., Mitchum., G. T., 2010. Estimating Mean Sea Level Change from the TOPEX and Jason Altimeter Missions Marine, Geodesy. 33(S1), 435–446. DOI: 10.1080/01490419.2010.491031

52. Nichols, M. N., 1989. Sediment accumulation rates and relative sea-level rise in lagoons, Marine Geology. 88, 201– 219.

53. Nicholls, R.J., Klein, R.J.T., Tol, R.S.J., 2007. Managing coastal vulnerability and climate change: a national to global perspective. In: McFadden, L., Nicholls, R.J., Penning-Rowsell, E. (Eds.), Managing Coastal Vulnerability. Elsevier, Oxford, UK, pp. 223–241.

54. Ojeda, J., 1988. Aplicaciones de la teledeteccion espacial a la din&mica litoral (Huelva), Geomorfologia y Ordenacion de1 Territorio. Ph.D. Thesis, University of Sevilla, Sevilla, pp. 411 (unpublished).

55. PALSEA (PALeo SEA level working group), 2010. The sea-level conundrum: case studies from palaeo-archives. Journal of Quaternary Science. 25**,** 19–25.

56. Pelling, H.E., Uehara, K., Green, J.A.M., 2013. The impact of rapid coastline changes and sea level rise on the tides in the Bohai Sea, China. J. Geophys. Res. Oceans, 118, 3462–3472. doi:10.1002/jgrc.20258.

57. Perillo, G.M.E., 1995. Definitions and geomorphological classifications of estuaries. In: Perillo, G.M.E. (Ed.), Geomorphology and Sedimentology of Estuaries. Developments in Sedimentology 53, Elsevier, Amsterdam, pp. 17 – 47

58. Pethick, J.S., 1994. Estuaries and wetlands: function and form. In: Falconer, R.A., Goodwin, P., (Eds) Wetland Management. Thompson Telford, London, 75–87.

59. Pfeffer, W.T., Harper, J. T., O'Neel, S. 2008. Kinematic constraints on glacier contributions to 21st-century sea-level rise. Science. 321, 1340–1343.

60. Pinto, L., 2003. Estrataficação salina no Estuário do Guadiana. Master thesis, Faculdade de Ciências da Universidade de Lisboa, Lisboa, pp. 179.

61. Plater, A., Kirby, J., 2006. The potential for perimarine wetlands as an ecohydrological and phytotechnological management tool in the Guadiana estuary, Portugal. Estuarine, Coastal and Shelf Science. 70, 98–108.

62. Prandle, D., 2004. How tides and river flows determine estuarine bathymetries. Progress in Oceanography. 61, 1–26. doi:10.1016/j.pocean.2004.03.001.

63. Prandle, D., 2009. Estuaries: Dynamics, Mixing, Sedimentation and Morphology. Cambridge University Press, New York, pp. 236.

64. Reeve, D., Chadwick, A., Fleming, C., 2004. Coastal Engineering processes, theory and design practice, Spon press, Oxon, United Kingdom, 461.

65. Sadler, P.M., 1981. Sediment accumulation rates and the completeness of stratigraphic sections. Journal of Geology. 89, 569–584.

66. Sadler, P.M., 1999. The influence of hiatuses on sediment accumulation rates. Geo Research Forum 5, 15–40.

67. Sampath, D.M.R., 2008. Impact of Shoreline Retreat and Inundation due to Sea-level rise along the Coastline adjacent to the Guadiana Estuary, Portugal/Spain Border, MSc. thesis, University of Alagarve, Portugal, pp. 93.

68. Sampath, D.M.R., Boski, T., Silva, P.L., Martins, F.A., 2011. Morphological evolution of the Guadiana Estuary and intertidal zone in response to projected sea-level rise and sediment supply scenarios. Journal of Quaternary Science. 26(2), 156–170. DOI: 10.1002/jqs.1434.

69. Sanford, L.P., Halka, J.P., 1993. Assessing the paradigm of mutually exclusive erosion and deposition of mud, with examples from upper Chesapeake Bay. Marine Geology. 114, 37–57.

70. Schubel J.R. 1971. Classification of estuaries. In: Schubel J.R. (ed.), Estuarine environment: estuaries and estuarine sedimentation Washington D.C., American Geological Institute. Cap. II, pp. 2–8.

71. Smith, S.V., 2005. Length of the Global Coastal Zone. In: Crossland, C.J., Kremer, H.H., Lindeboom, H.J., Marshall Crossland, J.I., Le Tissier, M.D.A. (Eds.), Coastal Fluxes in the Anthropocene. The Land–Ocean Interactions in the Coastal Zone Project of the International Geosphere–Biosphere Programme. Springer, New York, pp. 95–143.

72. Sommerfield, C.K., 2006. On sediment accumulation rates and stratigraphic completeness: lessons from Holocene ocean margins. Continental Shelf Research. 26, 2225–2240.

73. Stanford, J.D., Hemingway, R., Rohling, E.J., Challenor , P.G., Medina-Elizalde , M., Lester A.J., 2011. Sea-level probability for the last deglaciation: A statistical analysis of far-field records. Global Planet. Change**.** 79, 193–203.

74. Stevenson, J.C., Ward, L.G., Kearney, M.S., 1986. Vertical accretion in marshes with varying rates of sea level rise. In: Wolfe, D.A. (ed.), Estuarine Variability, Academic Press, San Diego, Calif , pp. 241– 259.

75. Stive, M. J. F., H. J. De Vriend, P. J. Cowell, and A. W. Niedoroda. 1995. Behavior-oriented models of shoreface evolution. Proceedings of Coastal Dynamics' 95, ASCE. 998–1005.

76. Stolper, D., 1996. The Impact of sea-level rise on estuarine mangroves: Development and Application of a Simulation Model. Honours Thesis, University of Sydney, Sydney, pp. 90.

77. Storms, J.E.A., Weltje, G.J., van Dijke, J.J., Geel C.R., Kroonenberg, S.B., 2002. Process-Response Modeling of Wave-Dominated Coastal Systems: Simulating Evolution and Stratigraphy on Geological Timescales. Journal of Sedimentary Research. 72, 226-239.

78. Syvitski, J.P.M., Harvey, N., Wolanski, E., Burnett, W.C., Perillo, M.E., Gornitz, V., 2005. Dynamics of the Coastal Zone. In: Crossland, C.J., Kremer, H.H., Lindeboom, H.J., Marshall Crossland, J.I., Le Tissier, M.D.A. (Eds.), Coastal Fluxes in the Anthropocene. The Land–Ocean Interactions in the Coastal Zone Project of the International Geosphere–Biosphere Programme. Springer, New York, pp. 39–94.

79. Townend, I., Pethick, J., 2002. Estuarine flooding and managed retreat Philosophical Transactions Royal. Society, London, 360, 1477–1495.

80. Townend, I., 2010. An exploration of equilibrium in Venice Lagoon using an idealised form model. Continental Shelf Research. 30 (8), 984–999 doi:10.1016/j.csr.2009.10.012

81. Valiela, I., 2006. Global Coastal Change. Water Framework Directive, 2000 (2000/60/EC)). Blackwell Publishing, Oxford pp. 368.

82. Vis, G., Kasse, C., Vandenbergue, J., 2008. Late Pleistocene and Holocene palaeogeography of the Lower Tagus Valley (Portugal): effects of relative sea level, valley morphology and sediment supply. Quaternary Science Reviews, 27, 1682-1709. DOI: 10.1016/j.quascirev.2008.07.003.

83. Ward, S.L., Green, J.A.M., Pelling, H.E., 2012. Tides, sea-level rise and tidal power extraction on the European Shelf. Ocean Dyn. 62, 1153–1167. doi:10.1007/s10236-012-0552-6.

84. Wolanski, E., Boorman, L.A., Chı´charo, L., Langlois-Saliou, E., Lara, R., Plater, A.J., Uncles, R.J., Zalewski, M., 2004. Ecohydrology as a new tool for sustainable management of estuaries and coastal waters. Wetlands Ecology and Management. 12, 235–276.

85. Wolanski, E., Chicharo, L., Chicharo, M.A., Morais, P., 2006. An ecohydrology model of the Guadiana Estuary (South Portugal) Estuarine. Coastal and Shelf Science. 70, 132–143.

86. Woodworth, P. L., 2010. A survey of recent changes in the main components of the ocean tide. Cont. Shelf Res. 30, 1680–1691. doi:10.1016/j.csr.2010.07.002.

87. Yue, T., Du, Z., Song, D., Gong Y., 2007. A new method of surface modelling and its application to DEM construction. Geomorphology. 91, 161–172.

88. Zazo, C., Dabrio, C.J., Goy, J.L., Lario, J., Cabero, A., Silva, P.G., Bardají, T., Roquero, E., 2008. The coastal archives of the last 15 ka in the Atlantic-Mediterranean Spanish linkage area: sea level and climate changes. Quaternary International, 181, 72–87. DOI: 10.1016/j.quaint.2007.05.021

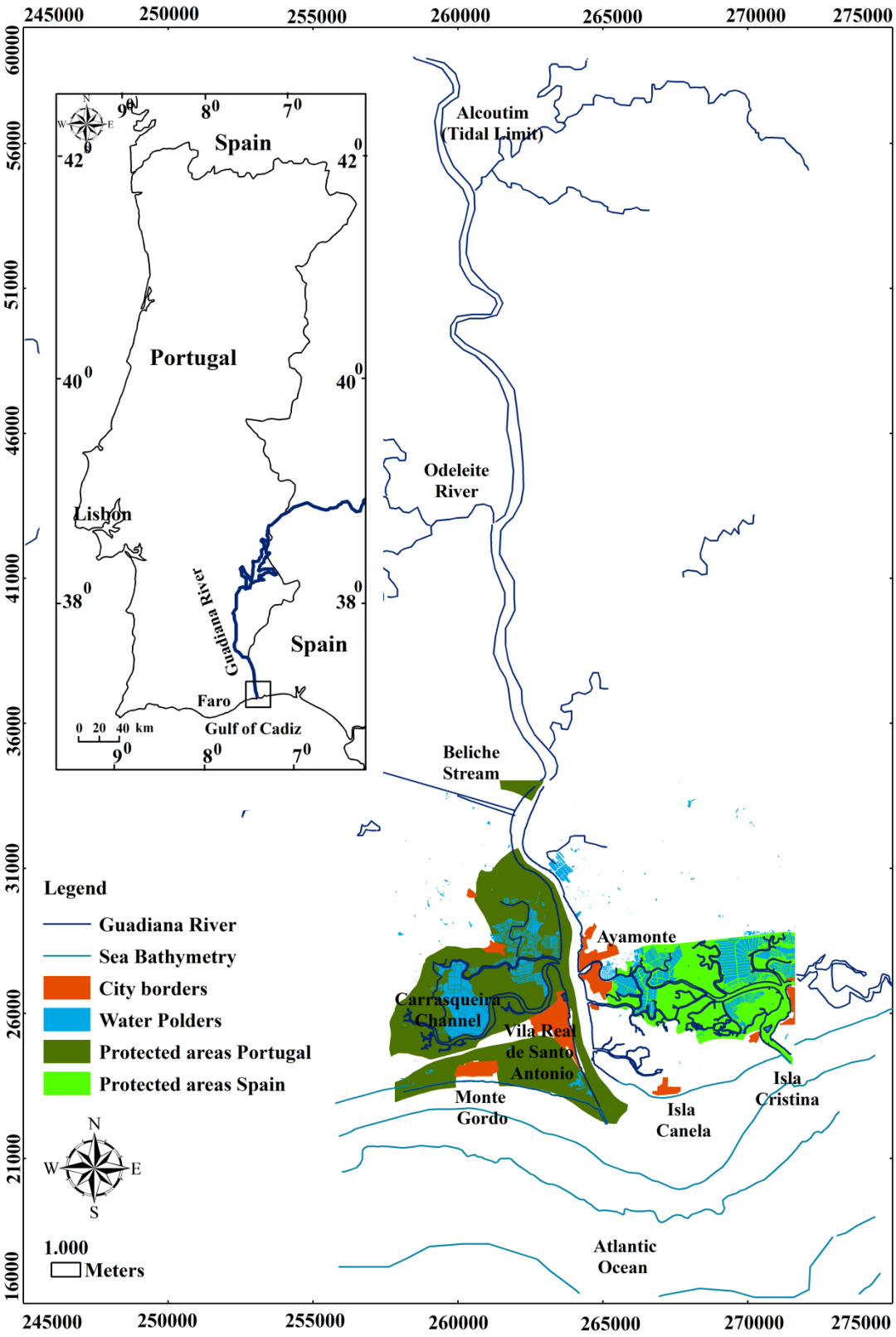

Note: The co-ordinate system is defined for the MEGASIG project (m)

Figure 1

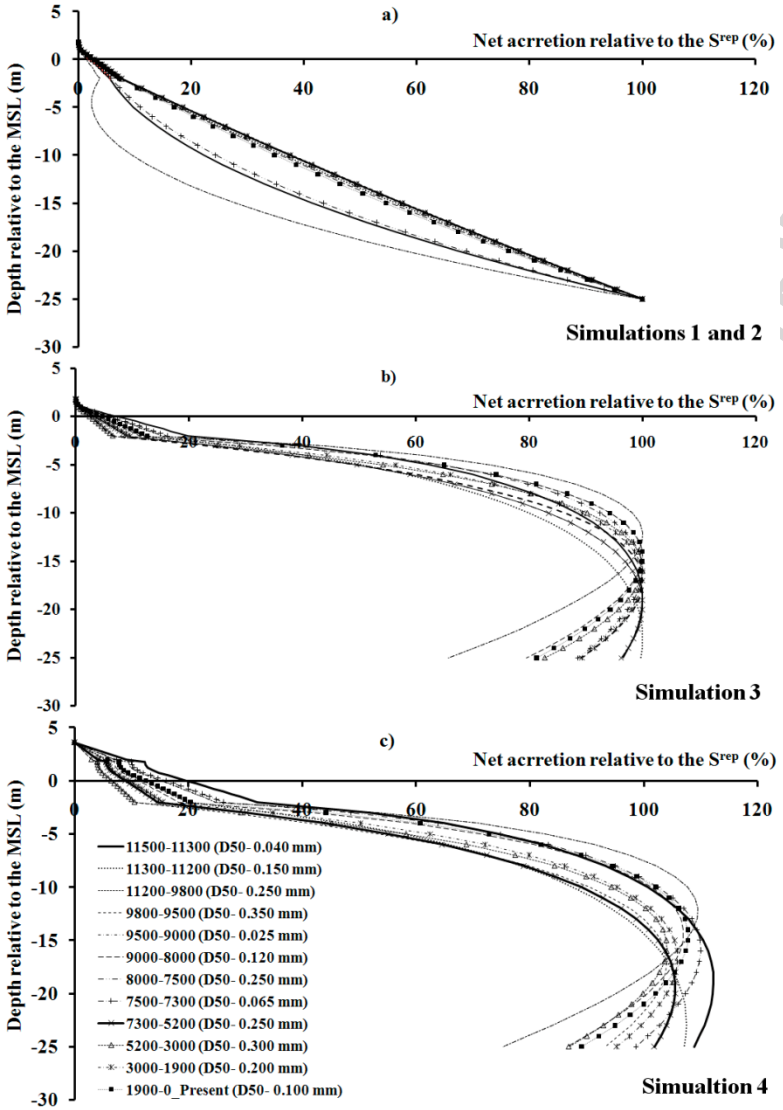

Figure 2

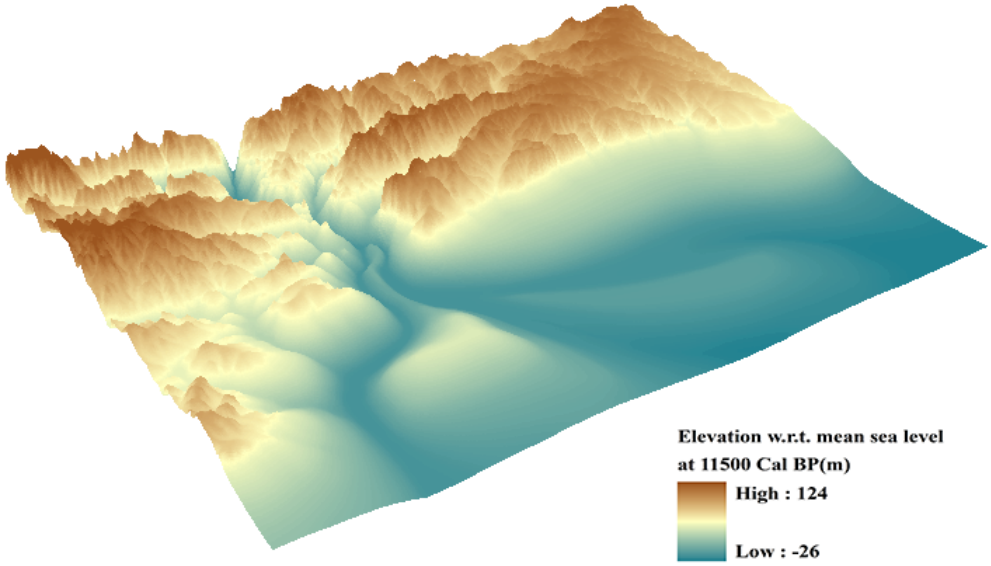

Figure 3

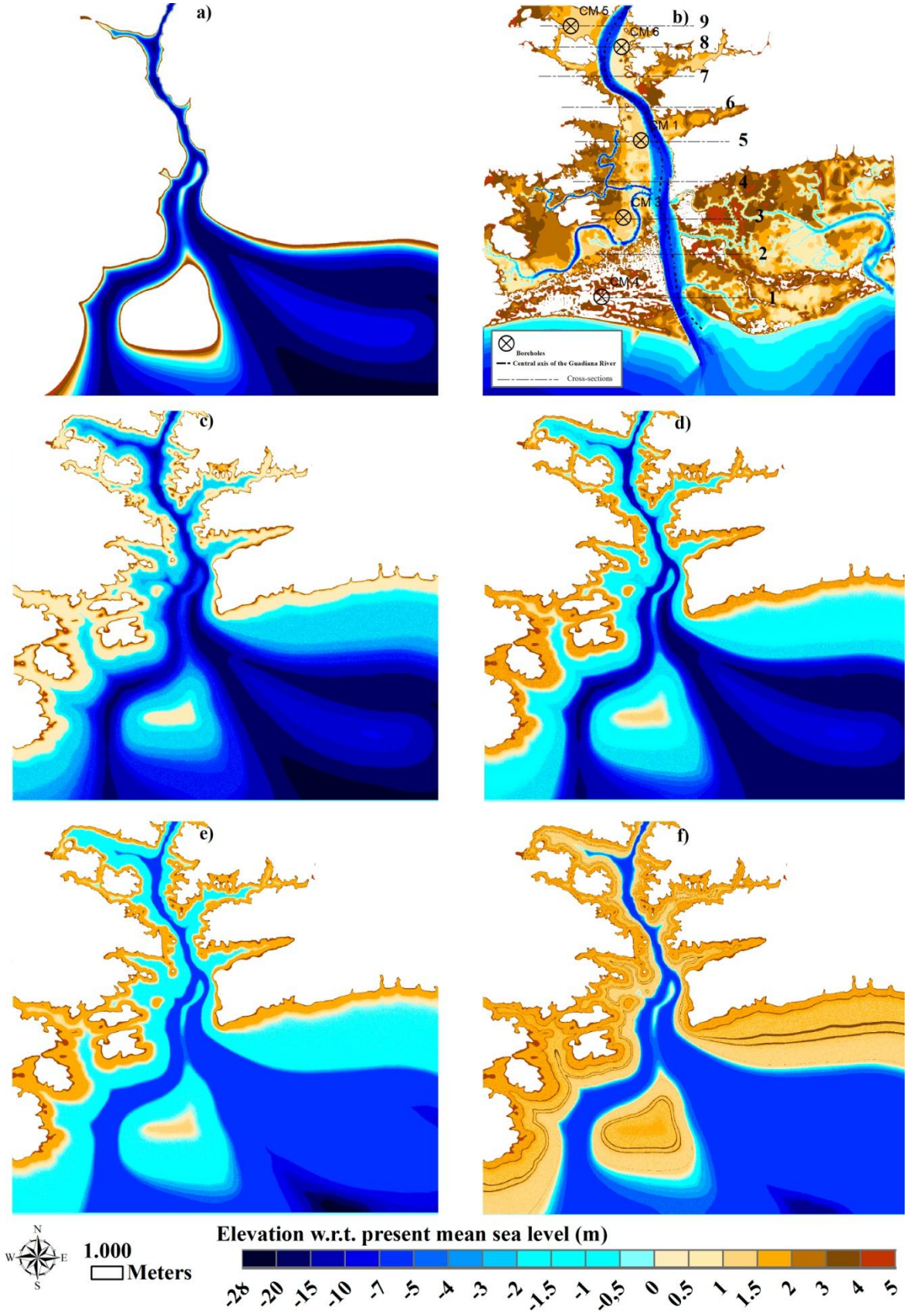

Figure 4

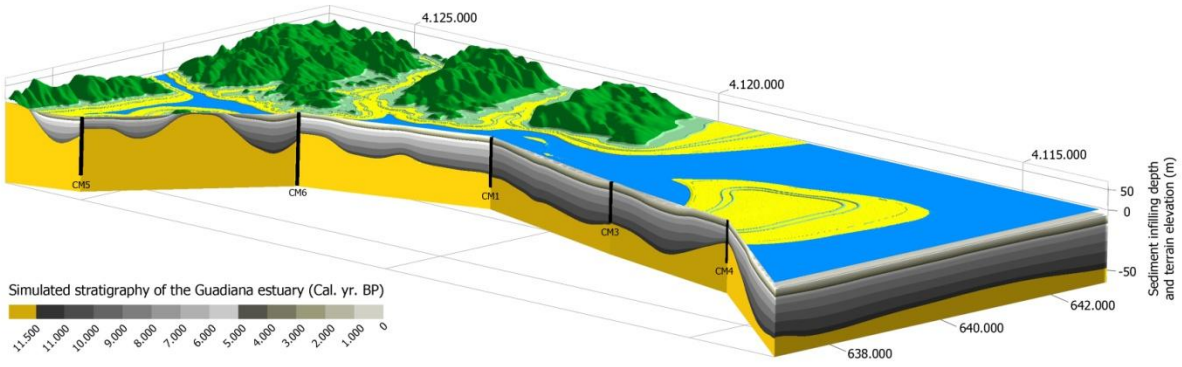

Figure 5

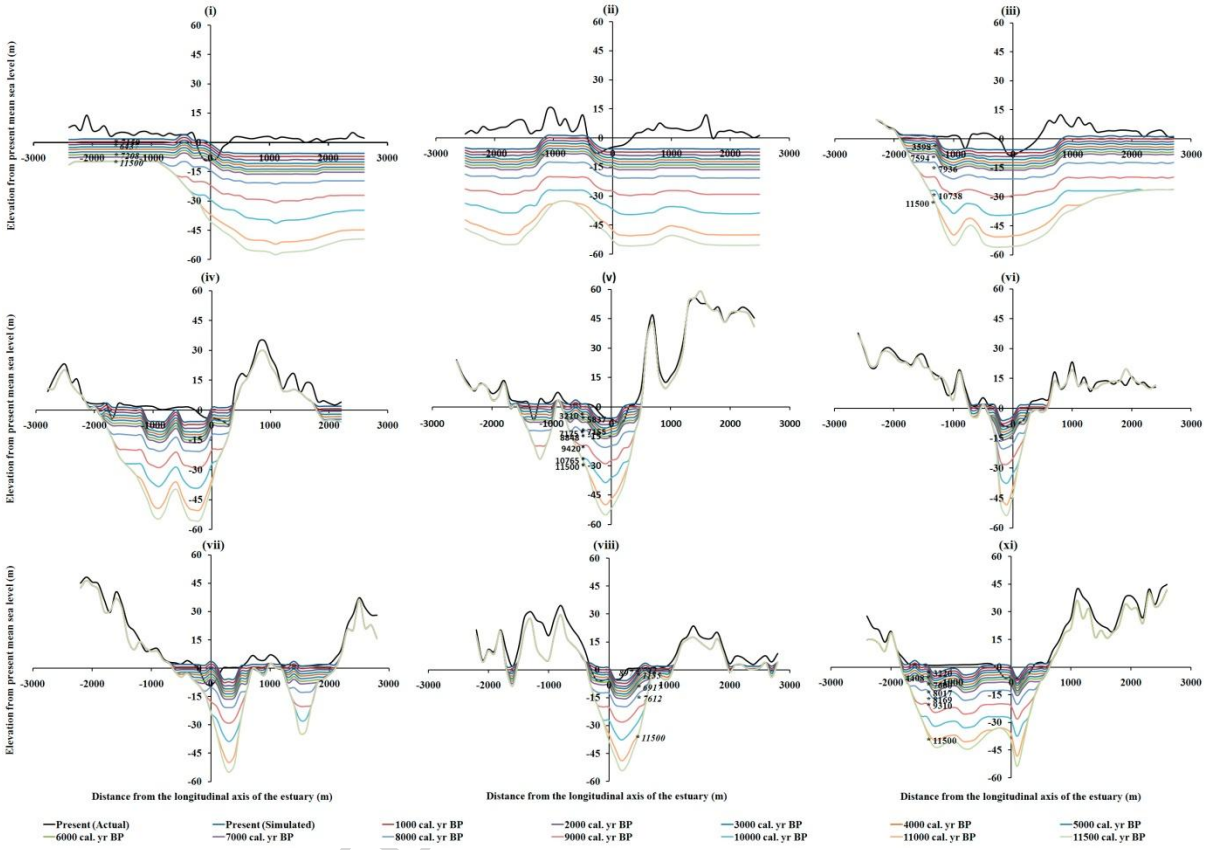

Figure 6

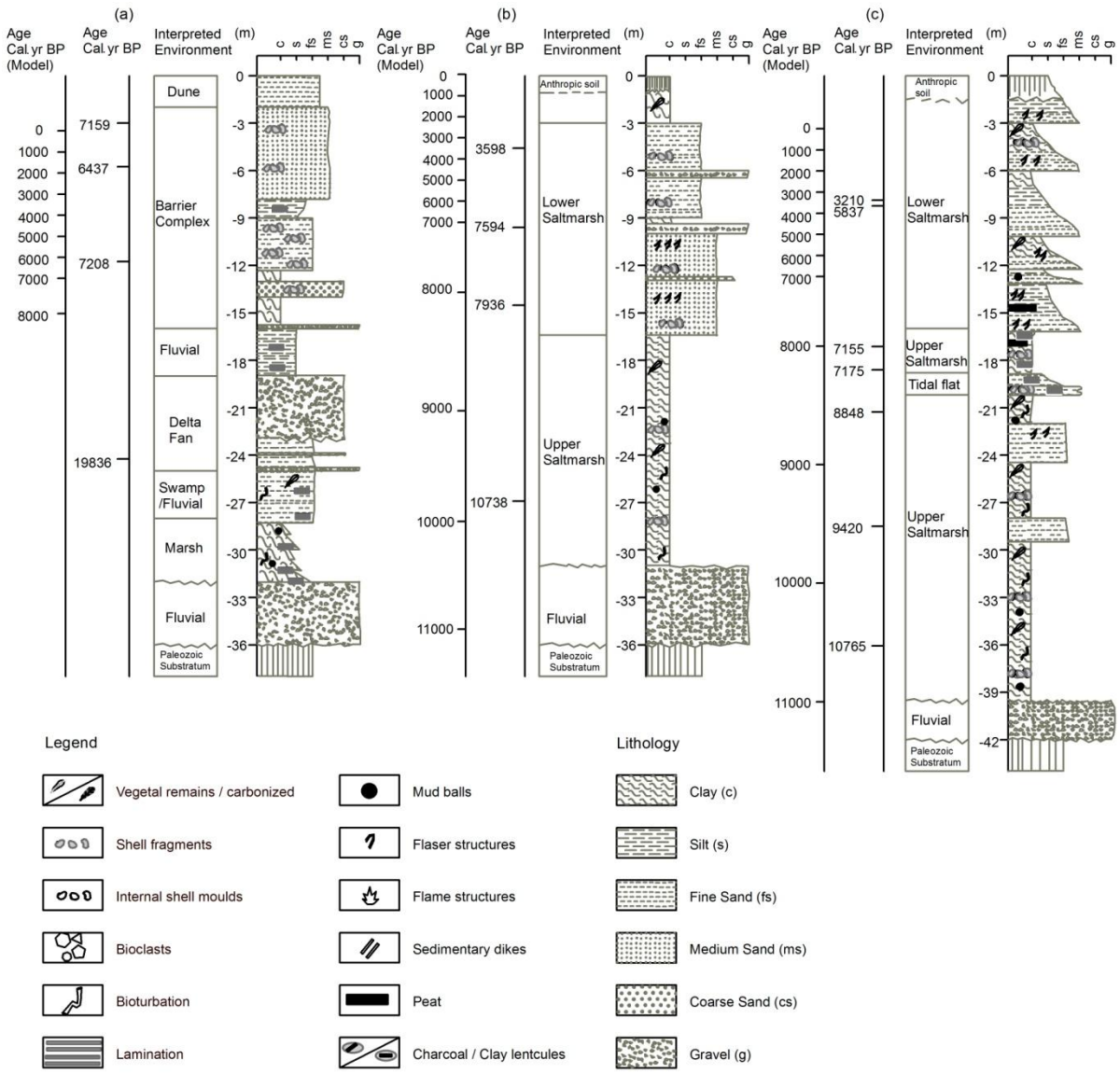

Figure 7

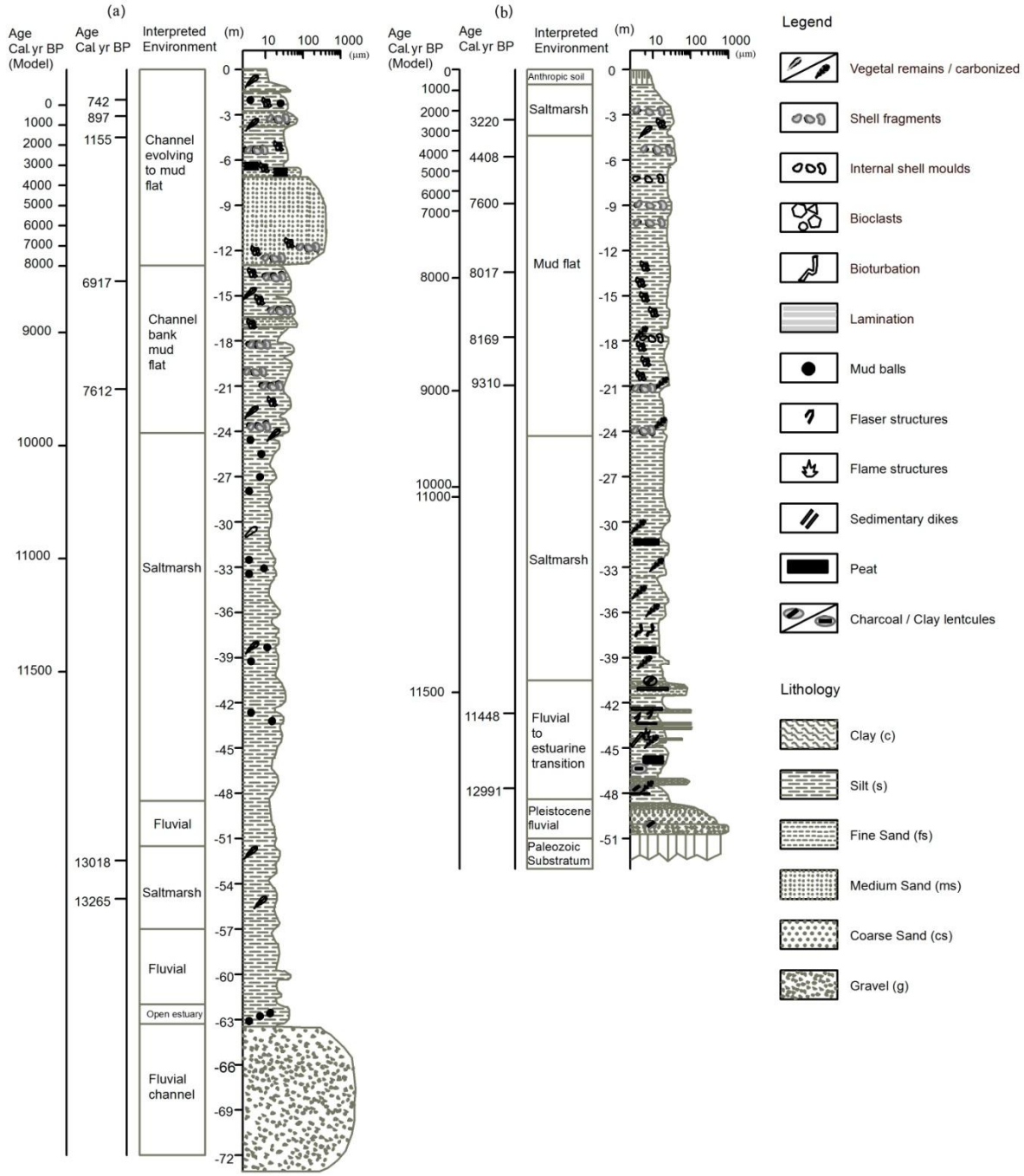

Figure 8

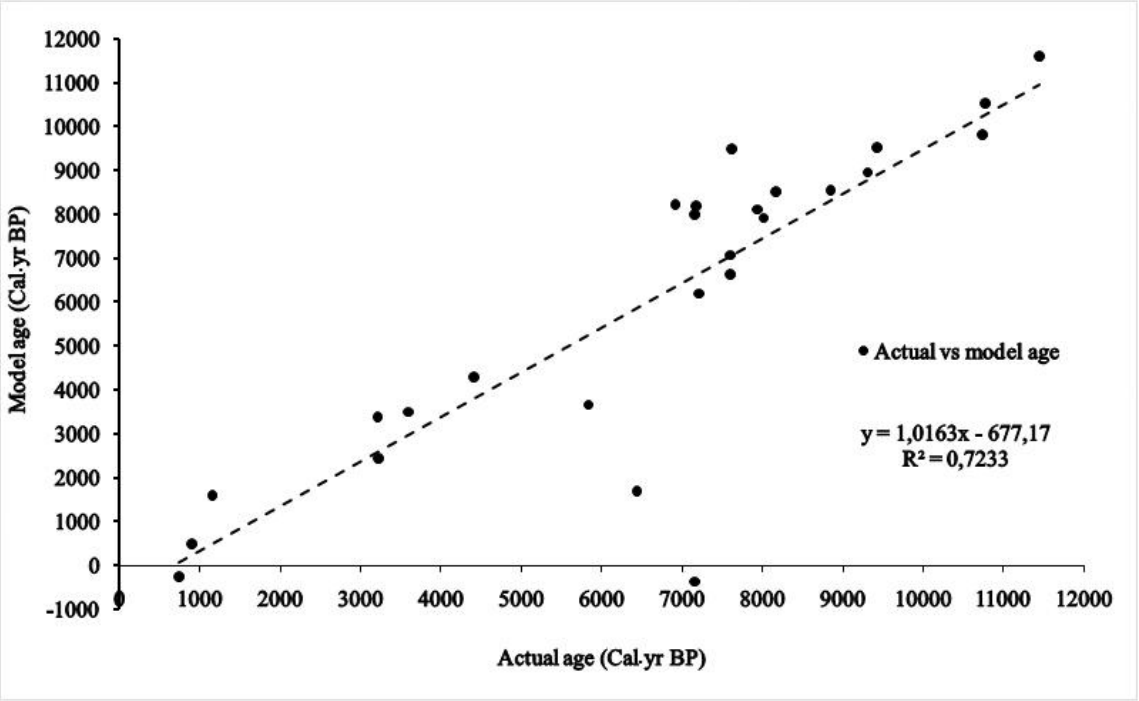

Figure 9

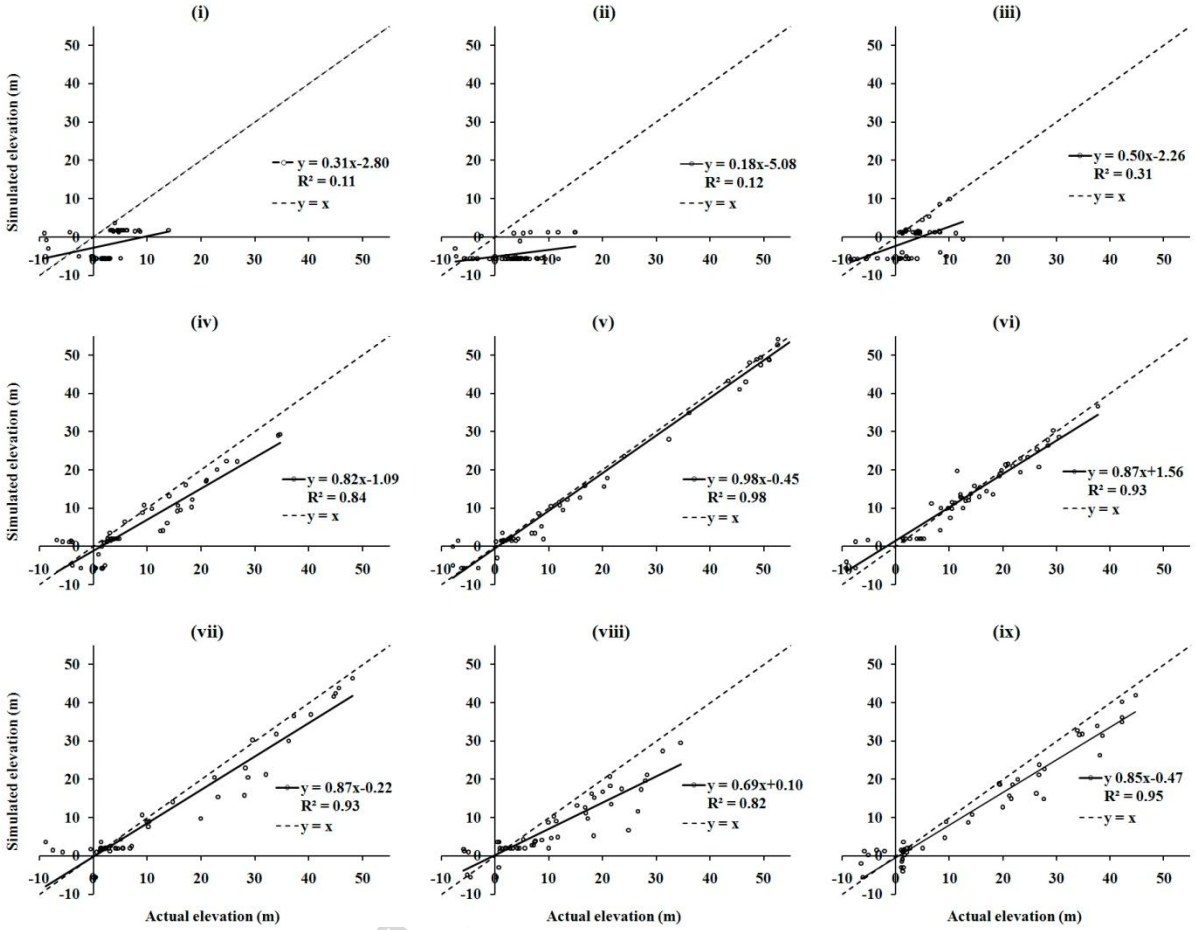

Figure 10

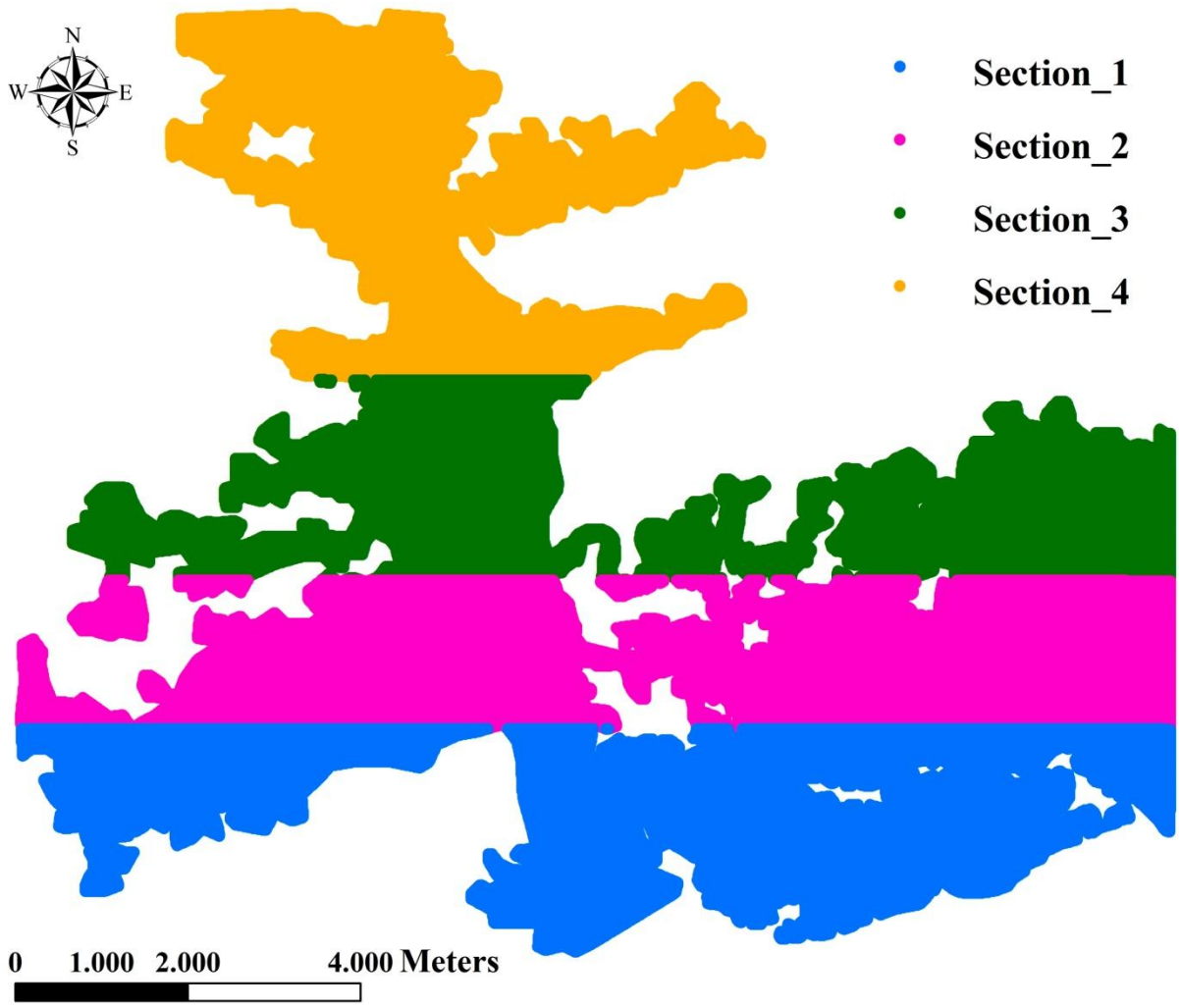

Figure 11

Tables

Table 1: Input data used to model Holocene sediment infilling in the Guadiana Estuary.

Simulation	Time (cal yr BP)	Set of net accretion curves (NAR)†	Sediment erosion coefficient (γ)	Sea-level rise rate (mm/yr) #	Sediment deposition rate (S^{Rep}) mm/yr
1	11500–7500 7500–0	1	$\gamma_1 = -2*10^{-7}z^2+9*10^{-6}-6*10^{-6}$	7.5 1.3	7.5§ 1.3§
2	11500–7500 7500–0	1	$\gamma_1 = -2*10^{-7}z^2+9*10^{-6}-6*10^{-6}$	7.5 1.3	8.5‡ 1.8‡
3	11500–7500 7500–0	2	$\gamma_2 = 6*10^{-8}z^2+7.8*10^{-6}+2.7*10^{-5}$	7.5 1.3	8.5‡ 1.8‡
4	11500–7500 7500–0	3	$\gamma_2 = 6*10^{-8}z^2+7.8*10^{-6}+2.7*10^{-5}$	7.5 1.3	8.5‡ 1.8‡

† See Figure 2.

Average value derived from data given by Boski et al. (2002) and Boski et al. (2008).

§ Derived from data given by Boski et al. (2008).

‡ Derived from data given by Boski et al. (2002).

Table 2: Summary information for ^{14}C age determinations showing conventional age, δ13C‰, 2 σ range and indicative ages used in the text and Fig. 6, 7, 8 and 9.

Borehole/ Sample	Depth MSL (m)	Material	Method	^{14}C Age (yr BP)	δ13C‰ (PDB)	Cal. yr BP 2σ		Indicative Age cal. yr BP
CM1.1	7.87	*C. glaucum*	AMS	3360 ± 31	0.64	3128	3332	3210
CM1.2	8.24	*C. glaucum*	β radiometric	5020 ± 310	1.1	4523	6028	5837
CM1.3	17.12	Peat	β radiometric	6210 ± 220	-25.9	6567	7560	7155
CM1.4	18.60	*C. edule*	AMS	6210 ± 40	2.08	6539	6765	7175
CM1.5	21.27	*C. angulata*	β radiometric	7590 ± 100	20	7855	8282	8848
CM1.6	28.50	*C. glaucum*	β radiometric	8430 ± 380	n/a	8153	10001	9420
CM1.7	36.06	*C. glaucum*	AMS	9500 ± 70	n/a	10209	10510	10765
CM3.1	4.59	*C. angulata*	β radiometric	3300 ± 160	n/a	2749	3496	3598
CM3.2	9.60	*C. angulata*	β radiometric	6710 ± 120	1.6	6951	7454	7594
CM3.3	14.52	*C. angulata*	β radiometric	7080 ± 200	0.7	7201	7951	7936
CM3.4	26.90	Wood	β radiometric	9470 ± 250	-22.9	9968	11601	10738
CM4.1	3.00	*V. nux*	β radiometric	6200 ± 340	1.6	5927	7377	7159
CM4.2	5.75	*S. plana*	β radiometric	5640 ± 90	-0.31	5866	6257	6437
CM4.3	11.75	*C. gibba*	β radiometric	6250 ± 250	1.4	6183	7265	7208
CM5.1	3.33	*S. plana*	AMS	3375 ± 39	-2.9 ± 0.2	3131	3354	3220
CM5.2	5.79	*Venerupis*	AMS	4295 ± 35	n/a	4295	4519	4408
CM5.3	8.90	*C. glaucum*	AMS	6764 ± 45	0.2 ± 0.2	7196	7401	7600
CM5.4	13.45	*Venerupis*	AMS	7585 ± 35	n/a	7958	8143	8017
CM5.5	17.75	*Cardium*	AMS	7725 ± 45	n/a	8063	8313	8169
CM5.6	20.95	Wood	AMS	8256 ± 55	-25.3 ± 0.2	9033	9423	9310
CM5.7	42.70	Wood	AMS	10273 ± 66	-25.5 ± 0.2	11768	12372	11448
CM5.8	47.67	Wood	AMS	10990 ± 40	-25.7	12857	13030	12991
CM6.1	2.00	Organic matter	AMS	830 ± 30	-28.1	686	789	742§
CM6.2	3.10	Organic matter	AMS	1000 ± 45	-31	792	981	897§
CM6.3	4.50	Organic matter	AMS	1215 ± 35	30.6	1059	1189	1155§
CM6.4	14.03	Peat	AMS	6060 ± 50	-25.96	6752	7155	6917§
CM6.5	21.2	*Venerupis*	AMS	7150 ± 50	-8.36	7518	7725	7612§
CM6.6	52.45	Wood	AMS	11110 ± 40	-28.9	12792	13131	13018§
CM6.7	55.00	Organic matter	AMS	11370± 50	-46.01	13125	13357	13265§

Note: § indicates the mean value (Delgado et al., 2012) while other indicative ages are median values (Boski et al., 2002; 2008)

Table 3: Comparison of root mean square errors on simulated water depths and corresponding actual depths and average errors on simulated accretion heights relative to those of actual accretion heights of the Guadiana estuarine system from 11,500 cal yr BP to the present.

Section	Number of bathymetric points	Root mean square error on simulated water depths (m)				Average error on simulated accretion relative to actual accretion (%)			
		Simulation				Simulation			
		1	2	3	4	1	2	3	4
1	175098	13.8	13.6	7.9	7.0	29.5	29.6	20.7	18.9
2	175113	9.7	9.2	5.6	4.9	35.8	35.4	30.2	28.5
3	147610	5.1	4.7	3.4	3.1	31.3	27.7	26.2	24.0
4	130000	4.5	4.2	3.5	3.7	47.5	42.9	42.3	41.9
Total	627821	8.7	8.3	5.3	4.8	35.6	33.5	29.1	27.5

Highlights

1. Morphological evolution of the Guadiana Estuary during the Holocene was modelled.
2. A behaviour-type estuarine sedimentation model was adopted for the simulations.
3. Sediment infilling in the estuary was simulated using a set of behaviour curves.
4. Behaviour curves reflect accretion rate coefficients dependent on estuary depth.
5. Simulations proved to be realistic for the sheltered environments of the estuary.